Pergamon

Geochimica et Cosmochimica Acta, Vol. 68, No. 19, pp. 3943-3969, 2004

0016-7037/04 $30.00 + .00

doi:10.1016/j.gca.2004.03.030

Chemical equilibrium and kinetic constraints for chondrule and CAI formation conditions

C. M. O'D. ALEXANDER*

Department of Terrestrial Magnetism, The Carnegie Institution of Washington, 5241 Broad Branch Road, Washington, DC 20015, USA

(*Received January* 22, 2003; *accepted in revised form March* 8, 2004)

Abstract—While many uncertainties remain, a kinetic evaporation-condensation model is used to show that type A chondrules, and compact Type A and B calcium-aluminum-rich inclusions (CAIs) could have formed from CI-like precursors under conditions that are consistent with predictions for 2–3 AU in a canonical solar nebula. Type B and Al-rich chondrules, and Type C CAIs, on the other hand, may have formed from fractionated precursors. Based primarily on chondrule and CAI isotopic compositions, previous studies have reached different conclusions because they did not take into account the effects of gas-melt exchange.

Assuming CI-like precursor compositions, equilibrium silicate melts with elemental compositions like those of type A chondrules could have formed over a wide range of conditions (T, P_{tot}, solid/gas/solar). Metal is not predicted to be stable when $T \geq 1600$°C. When $T < 1600$°C, the abundances and compositions of metal in chondrules appear to be less successfully reproduced than the silicates, e.g., at a given temperature more metal is predicted in type II chondrules than is generally observed, and under some conditions type IIs are predicted to be more metal-rich than type Is. These differences could be overcome if type Is formed from precursors that were more reduced than CI, and if type IIs formed after significant metal-silicate fractionation.

The formation conditions of molten CAIs are much more restricted than for chondrules, perhaps in part explaining their lower abundances. The Mg, Si and O isotopic mass fractionations in non-FUN CAIs can be reproduced if they formed between ~1400 to 1500°C in regions where CAI-like equilibrium melts were stable, but they did not quite reach equilibrium with the gas. CAI formation times at $P_{tot} = 10^{-4}$-10^{-3} bars are consistent with estimates of Type B CAI cooling times, but pressures much below this require formation times that are too long. The isotopic mass fractionations in FUN CAIs can be explained if they formed at or below the ranges of solid/gas/solar ratios where CAI-like equilibrium compositions are stable. Under these conditions, FUN inclusions undergo less gas-melt exchange than non-FUN CAIs. The FUN CAI formation temperatures are consistent with formation at 1400 to 1500°C, but may have been higher.

Two general explanations for the distribution of O mass independent fractionations (MIF) in chondrules/CAIs have been explored: creation of the MIF before chondrule/CAI formation, and creation of the MIF during chondrule/CAI formation. If the MIF was established before chondrule/CAI formation, the most promising explanation is that H_2O (presumably as ice) and silicate dust with MIFs of opposite sign are fractionated together from the remaining gas. On heating, the H_2O now in the gas exchanges with the melt.

If the MIF was generated during chondrule/CAI formation, it must be generated in the H_2O, because it exchanges most rapidly with the melt, and mass balance requires creation of MIF of opposite sign in CO. Self-shielding from UV radiation is one possibility, but the effect may be quenched at high temperatures. Non-RRKM intramolecular kinetic isotope effects are another possibility, but a continuous source of radiation may be needed to prevent gas phase reactions from approaching equilibrium. *Copyright © 2004 Elsevier Ltd*

1. INTRODUCTION

Chondrules and calcium-aluminum-rich inclusions (CAIs) are arguably the most important and are certainly the most studied objects in chondrites, yet their origins remain enigmatic. The textures of chondrules and a significant fraction of CAIs (Types B, C and compact Type As), as well as other types of inclusion (e.g., plagioclase olivine inclusions or POIs), show that they were largely molten when they formed. This implies that they experienced near liquidus peak temperatures. Liquidus temperatures for chondrules range from 1400 to 1800°C (Hewins and Radomsky, 1990) and for Type B CAIs peak temperatures of ~1400 to 1500°C have been inferred (Stolper, 1982; Stolper and Paque, 1986). The textures of chondrules and Type B CAIs have been used to estimate the cooling rates they experienced, which for chondrules are 5 to 1000°C/h (Hewins, 1988; Jones and Lofgren, 1993; Lofgren, 1996) and for Type B CAIs 0.5 to 50°C/h (MacPherson et al., 1984; Stolper and Paque, 1986).

Both chondrules and CAIs are thought to have formed in the nebula. Given the low pressures this would imply, as well as the high temperatures and the relatively modest cooling rates that they experienced, it seems inevitable that they would have experienced some evaporation during heating and condensation during cooling. Evaporation and condensation are generally accompanied by isotopic mass fractionation–evaporation enriches the residue in heavy isotopes, while condensation enriches the condensate in the light isotopes relative to the gas.

There is clear isotopic evidence for evaporation and condensation in the molten CAIs. Most molten CAIs exhibit isotopic mass fractionation in one or more of the elements Mg, Si, O, Ca and Ti (Clayton et al., 1988). However, the senses of the mass fractionations in these elements are not always the same, indicating that these CAIs experienced complex histories of evaporation and condensation. The Mg and Si isotopic fractionations are highly correlated, but the relative fractionations are

* Author to whom correspondence should be addressed (alexande@dtm.ciw.edu).

not what is observed in evaporation experiments using solar initial compositions (Wang et al., 2001). This has lead to the conclusion that the precursors of the molten CAIs were not solar, but were more refractory and/or that these CAIs formed under non-Rayleigh conditions (Grossman et al., 2000; Richter et al., 2002). These conditions may have included high nebula pressures ($P_{tot} > 10^{-3}$ bars), when fast evaporation rates, combined with relatively slow diffusion in the melt and the gas, reduced the isotopic fractionation during evaporation.

Many features of chondrule bulk compositions can be explained by evaporation (Jones, 1990; Sears et al., 1996; Cohen et al., 2000). Yet, there is remarkably little isotopic mass fractionation in chondrules compared to what would be expected if their range of elemental compositions were produced by evaporation of an initially "solar" composition melt under Rayleigh conditions. The range of reported isotopic mass fractionations or upper limits for mass fractionations in chondrules are: K < 1–2‰/amu (Alexander et al., 2000; Alexander and Grossman, 2000); Fe, <1‰/amu (Alexander and Wang, 2001), ~0.5‰/amu (Zhu et al., 2001), ~0.15‰/amu (Kehm et al., 2003), ~1.1‰/amu (Mullane et al., 2003); Si, ~0.5‰/amu (Clayton et al., 1991); Mg, 1‰/amu (Galy et al., 2000; Nguyen et al., 2000).

Galy et al. (2000) report very modest fractionations of Mg isotopes in a suite of Allende chondrules with a wide range of Mg/Al ratios. They suggest that the chondrules formed at high partial pressures of hydrogen, possibly as high as 1 bar. Under these conditions, evaporation would have occurred far from Rayleigh conditions and isotopic fractionations associated with evaporation would have been suppressed.

However, most astrophysical models predict ambient midplane pressures well below $P_{tot} = 10^{-4}$ bars at 2–3 AU (Boss, 1996). Massive disks ($\geq 0.1 M_o$) that would produce midplane pressures that approach $P_{tot} = 10^{-4}$ bars are likely to be gravitationally unstable (Boss, 2000) and are rare, at least around T Tauri stars (Beckwith et al., 1990). Shock waves can temporarily increase gas pressures by 1–2 orders of magnitude (Desch and Connolly, 2002). A $P_{tot} = 10^{-3}$ bars is therefore a likely upper limit if chondrule and/or CAI formation took place in the asteroid belt. If chondrules and/or CAIs formed at $P_{tot} > 10^{-3}$, they either formed much closer to the Sun (<1 AU) or, if pressures of ~1 bar are required (Galy et al., 2000), they formed in a nonnebular setting. Either explanation would have profound implications for our understanding of nebula evolution and chondrite formation.

An alternative explanation for chondrules' lack of isotopic fractionation is that they formed under more canonical nebula pressures ($P_{tot} \leq 10^{-3}$ bars), but after an initial period of evaporation they equilibrated with the ambient gas (Alexander et al., 2000; Alexander and Wang, 2001).

One other important feature of chondrules and CAIs that must be explained by any complete model for their formation are their so-called mass independent isotope fractionations (MIFs) in O. The origin of these anomalies has been a mystery since their discovery (Clayton et al., 1973). The original explanation for the MIF was that chondrule and CAI precursors included variable amounts of ^{16}O-rich supernova condensates. However, this has been all but ruled out by the fact that supernova condensates are only a minor component of presolar oxide (Nittler et al., 1997; Choi et al., 1998; Nittler et al., 1998) and silicate grains (Messenger et al., 2002). At present, the best explanation for the MIF anomalies is that they were produced by gas-chondrule/CAI exchange (Thiemens, 1988; Clayton, 1993). The MIF between the gas and the chondrules/CAIs could have been established either before or during chondrule/CAI formation.

Here a kinetic model that follows the elemental and isotopic fractionations during metal-silicate evaporation-condensation is used to place some first order constraints on the conditions of chondrule/CAI formation, as well as the nature of the O reservoirs and possible mechanisms responsible for the O MIF.

The aim of this paper is to explore whether chondrules and the molten CAIs could have formed by melting and evaporation of solar composition precursors followed by partial or complete reequilibration with the gas under conditions that are consistent with a canonical solar nebula ($p = 10^{-6}$-10^{-3} bars, solar bulk composition, but with local dust+protochondrule/CAI enrichments and depletions). This is a somewhat different approach to previous equilibrium condensation studies which envisaged that all material evaporated and then condensed under equilibrium conditions (Grossman, 1972; Wood and Hashimoto, 1993; Yoneda and Grossman, 1995; Ebel and Grossman, 2000). The range of conditions (temperature, pressures and dust enrichments) explored span a likely range for chondrule/CAI formation. The elemental and isotopic compositions that develop under these conditions, as well as the times needed to produce them, are compared to the compositions of chondrules/CAIs and to the formation timescales that have been inferred for them. Along with the rates for gas-gas and gas-melt exchange, these results are also used to test various models for producing the O MIF.

2. SUMMARY OF KINETIC MODELS

Alexander (2001, 2002a) presented two models, named PCR and EQR, for estimating evaporation rates. They are both quite successful at reproducing various free evaporation experiments, but they do predict rather different evaporation/condensation rates under nebular conditions. Results for both models are presented here to illustrate some of the uncertainties inherent in the calculations. Many details of the evaporation-condensation models have been described previously (Alexander, 2001, 2002a), although some important modifications are described in an electronic annex (EA1, EA2). Here the most important features of the models are summarized.

Heating and cooling of the dust and gas assemblage is assumed to occur in a closed system at constant pressure, i.e., upon heating and as material evaporates the system expands and during cooling it contracts, but there is no net change in its bulk composition.

2.1. Evaporation-Condensation Rates

Both models calculate maximum evaporation rates and are then calibrated by comparison with experimentally measured free evaporation rates. In the EQR model, the maximum evaporation rates are calculated from the equilibrium partial pressures of the melt (e.g., the equilibrium partial pressure of $Mg_{(g)}$ for evaporation of MgO). Maximum condensation rates are based on the partial pressures of reactants (e.g., $Mg_{(g)}$) in the

nebula gas. Evaporation/condensation can occur via a number of different reactions involving O/O_2, H/H_2-H_2O, H/H_2-OH, and CO-CO_2. In some models for the origin of MIF, these gases may have very different O isotopic compositions. Therefore, the rates for the individual reactions need to be known. In the EQR model, the relative rates of these different reactions are estimated from the relative abundances of O, O_2, H_2O, OH and CO_2 in the equilibrium vapor of the melt (evaporation) or in the nebula gas (condensation).

The PCR model calculates the maximum evaporation-condensation rates of the individual evaporation/condensation reactions based on the stoichiometry of the gas and the Gibbs free energy changes of the reactions, the activities of the components in the melts (evaporation) and the partial pressures of the reactants (condensation).

Accurate activities of components in the melt are essential for calculating evaporation rates in both kinetic models. For CaO-MgO-Al_2O_3-SiO_2 (CMAS) liquids, activities are calculated using the solution model of Berman (1983). For FeO-bearing melts, the activities are calculated using the MELTS model (Ghiorso and Sack, 1995). The accuracy of the activities calculated with these two models for the melt compositions encountered here is not known. For the Fe-Ni-S system, the solution model of Hsieh et al. (1987) is used. Thermodynamic data for most gases are from Knacke et al. (1991). For those gases not included in the Knacke et al. compilation, the thermodynamic data were taken from Chase (1998). The melt densities, used to determine the sizes of the chondrules/CAIs, are calculated with the model of Lange and Carmichael (1987).

The calculated maximum evaporation rates are compared to experimentally determined free evaporation rates. Differences between the calculated and measured rates are accounted for with so-called evaporation (α) coefficients. Condensation rates are much more difficult to measure, and condensation coefficients have yet to be determined for most systems. In order that at steady state the system reaches the predicted thermodynamic equilibrium conditions, the free evaporation and condensation coefficients are assumed to be identical. In the PCR model, the composition of the ambient gas can cause evaporation and condensation rates to be suppressed, particularly near equilibrium when gas pressures are relatively high. If the gas suppression coefficient is less than the free evaporation/condensation coefficient, the gas suppression coefficient is assumed to control the rates.

The free evaporation coefficients for $MgO_{(l)}$, $SiO_{2(l)}$ and $FeO_{(l)}$ have been estimated from several sets of vacuum evaporation experiments conducted at temperatures between 1700°C and 2000°C. The coefficients are simple functions of temperature only, despite large changes in composition during the experiments. Recent experiments using CAI-like initial compositions (Richter et al., 2002; Richter, personal communication) suggest that extrapolations of the functions down to 1600°C are reasonably accurate, as long as the MgO mole fraction is above a temperature dependent critical value (see electronic annex, section EA2).

Very few evaporation experiments have been conducted in the presence of hydrogen. One recent set of experiments conducted on CAI-like melts at 1500°C and $pH_2 = 1.87 \times 10^{-4}$ atm. (Richter et al., 2002) provide estimates of the free evaporation coefficients for MgO and SiO_2 reactions involving hydrogen (see section EA2). For the PCR model, for instance, the free evaporation coefficients are 0.25 times those predicted by the vacuum coefficients. There has been no experimental determination of evaporation rates in the presence of hydrogen for FeO or for any other chondritic melt components. The hydrogen α coefficients for all components and all conditions are estimated by assuming that they all have the same ratio of vacuum/hydrogen free evaporation coefficients as MgO and SiO_2 in these experiments.

Evaporation coefficients for Fe-Ni-S melts have yet to be measured. They have been measured for solid Fe and Ni, and are close to unity (Xiong and Hewins, 2000, 2001). Since kinetic barriers are likely to be higher for solids than liquids, assuming evaporation coefficients of one for Fe-Ni-S melts seems justified.

2.2. Melting, Metal-Silicate Segregation, Etc.

As stated earlier, the aim of this paper is to follow the elemental and isotopic evolution of solar composition material upon heating. If temperatures rapidly rise above the solidus temperature of the precursor material, it will partially or completely melt. It will also begin to evaporate and later begin reequilibrating with the gas. Although the model can simulate melting/dissolution and crystallization, they are not included here for two reasons. First, quantitatively the rates of nucleation, growth-dissolution and diffusion as a function of temperature, mineral/melt composition, etc. are generally not well understood. Second, the initial compositions, sizes and abundances of minerals can have an influence on the subsequent evolution of the mineral-melt system, and we know very little about the initial state of the chondrule/CAI precursors. Thus, the inclusion of dissolution-crystallization would potentially introduce additional uncertainties into the calculations that are unwarranted at this stage. Nevertheless, given that crystal growth, dissolution and equilibration etc. are not instantaneous processes, the first order evaporation and equilibration timescales presented here are probably minimum estimates.

Many chondrules (e.g., barred olivine chondrules) and CAIs were largely or wholly molten near their peak formation temperatures, when most evaporation would have taken place. Hence, for these first order calculations ignoring melting/dissolution and crystallization is justifiable. Past studies have assumed that thermodynamic equilibrium is always maintained (Grossman, 1972; Wood and Hashimoto, 1993; Ebel and Grossman, 2000). However, numerous features of chondrules and CAIs indicate that they are not equilibrium assemblages (presence of glass, zoned minerals, disequilibrium textures, isotopic mass fractionation, etc.). Therefore, modeling them by assuming that equilibrium is always maintained is also only an approximation. As will be shown later, whether or not crystallization is included does not make a large difference to the bulk equilibrium compositions. However, crystallization/dissolution is likely to increase timescales of evaporation and reequilibration, as well as modify the compositional paths of chondrules/CAIs as they evolve towards equilibrium with the gas.

Upon heating, Fe-Ni-S and silicate melts are assumed to form separate objects whose relative sizes are proportional to their initial relative abundances and densities. This avoids uncertainties in how to treat a chondrule/CAI melt composed of

two intimately mixed immiscible liquids. Since Fe-Ni-S blebs in a chondrule would not be able to efficiently "communicate" with one another via diffusion, they would have to be modeled individually, which would be impractical and would require too many assumptions (e.g., how they grow when they encounter one another, how they migrate to the surface, etc.).

Diffusion, either in the melt or in the gas, is assumed not to have any influence on evaporation or condensation. At the still modest pressures assumed here and for objects that are up to a few millimeters across, this is probably a good assumption. However, for larger objects and at pressures above 10^{-3} bars, the influence of diffusion in both the melt and the gas are likely to become increasingly important (Richter et al., 2002).

Isotopic exchange between gas and melt only occurs via evaporation-condensation reactions. Direct exchange (e.g., $H_2{}^{16}O_{(g)} + {}^{18}O_{(l)} = H_2{}^{18}O_{(g)} + {}^{16}O_{(l)}$) is not considered because the sticking coefficients for these reactions have not been determined.

Chemical and isotopic equilibration in the gas phase occurs via a suite of 31 gas phase reactions (see Table EA2). For reactions involving at least two O atoms, mass independent isotopic fractionation of the O can be included. This is done by assuming that the rate coefficient for a reaction involving ^{16}O atoms only is faster than for all other reactions. How much faster the ^{16}O-^{16}O rate coefficient is, is a free parameter. The rate coefficient for the reverse reaction is enhanced to the same degree.

2.3. Comparison with Previous Work

The bulk compositions of "equilibrium" melts (ignoring crystallization) can be approximated by integrating the models for long times so that they approach a steady state. Comparison with the work of Ebel and Grossman (2000) shows that, at least under these conditions, "equilibrium" melt compositions are not very different from the bulk compositions of equilibrium condensates (Fig. 1). This is because in general the free energy difference between a mineral/melt assemblage and a melt of the same bulk composition is not very large.

Of the major and minor elements considered here, the alkalis are the most affected by whether or not crystallization is allowed—no crystallization suppresses their condensation temperatures. However under the conditions explored here, there is not significant condensation of the alkalis even when crystallization is included (Ebel and Grossman, 2000). Barring significant errors in the alkali activities predicted by MELTS, it appears that the alkalis either condensed and diffused into the chondrules at lower temperatures in the nebula than considered here, and/or entered chondrules during parent body processing (Grossman et al., 2002; Grossman and Brearley, 2003).

The next most crystallization sensitive component is FeO. In Figure 1, the FeO contents are somewhat overestimated at a dust enrichment of 1000 times solar and at temperatures below 1800 K. For 100 times solar dust enrichment and temperatures below 1700 K, the FeO contents are about half the already low abundances predicted if there is crystallization.

2.4. Range of Conditions

The aim of the paper is to identify the range of conditions where chondrules and CAIs could have formed if the initial composition of the precursors were CI-like. To make the problem tractable, the number and range of parameters that are explored are necessarily restricted. The range of conditions explored were: constant total pressures of 10^{-4}, 2.5×10^{-4}, 5×10^{-4}, 7.5×10^{-4} and 10^{-3} bars, constant temperatures of 1400°C, 1500°C, 1600°C and 1700°C, and a total range of solid/gas enrichments relative to solar of 10 to 60,000. Solid/gas rather than dust/gas is used to avoid confusion because only roughly millimeter-sized objects are assumed to be present. The pressures are at the upper end of estimates for the canonical solar nebula, even when enhanced by the passage of shock waves. The temperatures span most of the range of liquidus temperatures for chondrules and Type B CAIs. More detailed studies including variable heating and cooling rates, variables pressures, precursor mineralogy and grain size, crystallization etc. will have to be done, but given the huge potential phase space, these will almost certainly have to be done in the context of specific models (e.g., Desch and Connolly, 2002).

2.5. Initial Solid and Gas Compositions

The solar composition used was that of Anders and Grevesse (1989). Recently, Allende Prieto et al. (2001, 2002) have reported significantly lower solar photosphere O and C abundances, although their ratio remains similar to that of Anders and Grevesse (1989). The new abundances bring the solar composition more in line with astronomical estimates for young stars and interstellar material in the solar neighborhood. The effect of these lower O and C abundances mean that the dust enrichments needed to stabilize a melt of a given composition would have to be higher than if the Anders and Grevesse (1989) solar composition is used.

Alexander (2002b) and Ebel and Alexander (2002) have argued that cluster IDPs, with or without ice, are a better analog for the primordial dust than CI chondrites. This is because CI chondrites have been completely aqueously altered on their parent body and, in the process, heavily oxidized. Cluster IDPs contain circumstellar and interstellar material (Messenger and Walker, 1997; Bradley et al., 1999; Messenger et al., 2002), little or no FeO, and are C-rich. Even very modest enrichments of dust of this composition produce conditions that are reducing enough to create enstatite chondrite-like mineral assemblages (Ebel and Alexander, 2002). To produce relatively oxidizing conditions, ice must accompany the dust. The evidence of aqueous alteration in almost all chondrite classes suggests that ice was probably present throughout much of the asteroid belt at the time of planetesimal accretion (Alexander et al., 2001). The ice condensation front, or snow line, would have been somewhere between the formation locations of the enstatite and ordinary chondrites. Midplane temperatures at 2–3 AU in T Tauri disks are commonly low enough for ice condensation (Woolum and Cassen, 1999). If chondrules formed shortly before or contemporaneously with the planetesimals, ice would have been present when they formed.

The silicate/ice ratio would introduce another free parameter. For this reason, as well as to make comparisons with previous work easier, a CI-like dust composition is used. Nevertheless,

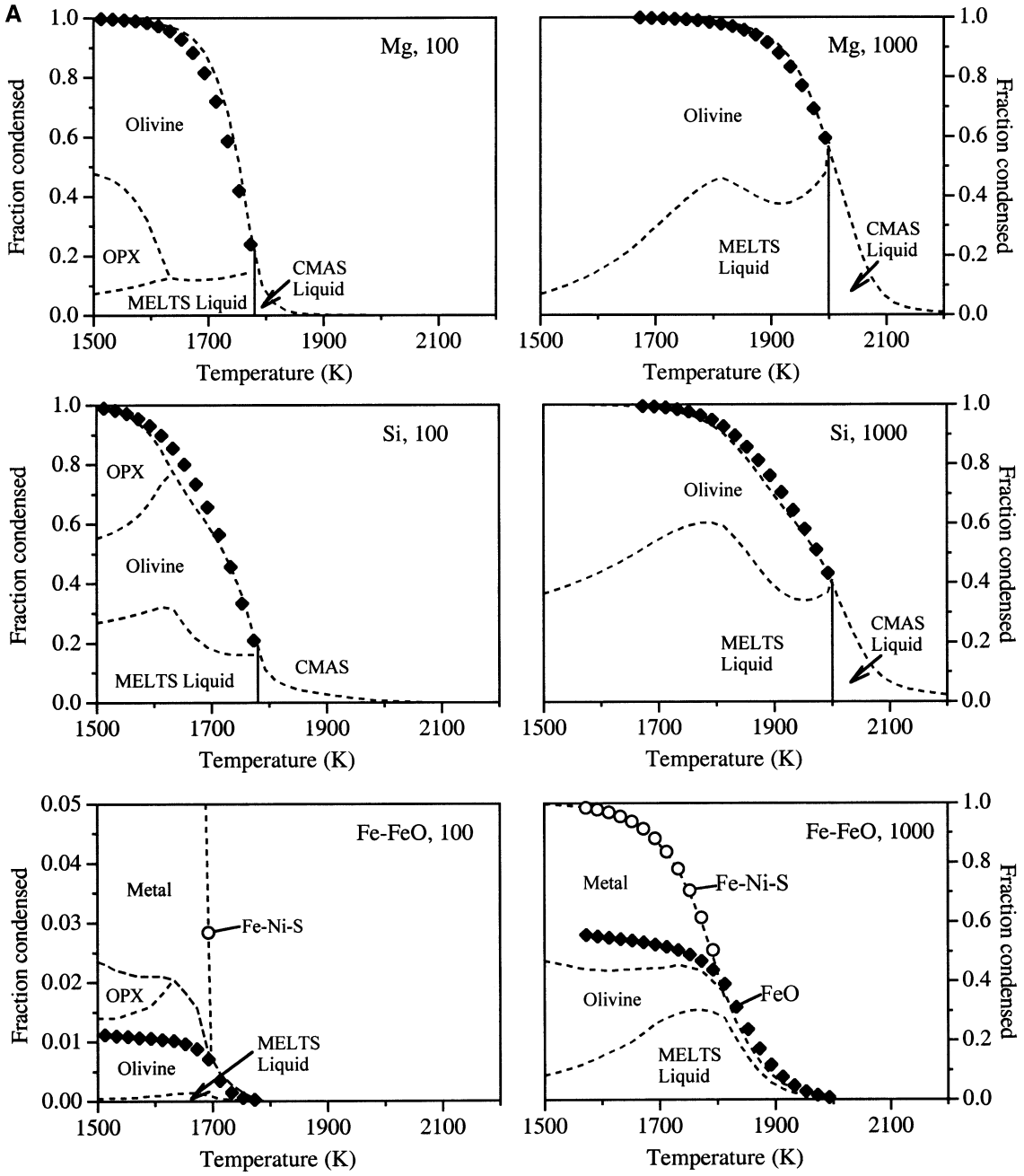

Fig. 1. (a) Comparison of the bulk equilibrium compositions calculations by Ebel and Grossman (2000) and in this work (symbols). The filled symbols are for the silicate melt, and the open symbols are for the Fe-Ni-S melt. The conditions were a total pressure of 10^{-3} bars with 100 and 1000 times solid/gas/solar enrichments. Ebel and Grossman (2000) included crystallization, but only melts were considered in this work. Nevertheless, the results of the two studies are very similar. The results from this work are not shown when only CMAS liquids are predicted by both approaches since they are identical. (b) Comparison of the equilibrium bulk Ni-content of metal alloy (Ebel and Grossman, 2000) and of Fe-Ni-S melt (symbols) under the same conditions as in (a). The lower Ni contents of the melt below ~1600 K in the solid/gas/solar = 1000 calculations are due to condensation of S.

the precursor material is assumed to be anhydrous, all S is assumed to be present as FeS, a small amount of Fe is converted to metal along with all Ni, and all remaining Fe is taken to be FeO (Table 1). This produces a considerable amount of excess O associated with H_2O/OH, sulfate, magnetite and carbonate. Excess O (henceforth "volatile" O) and all C are assumed to evaporate instantaneously on heating without producing any isotopic fractionation of the O. Cluster IDPs contain little or no FeO. If the primordial dust was like cluster IDPs, the calculated Fe and O isotopic mass fractionations during evaporation will be overestimates because of the fractionation associated with FeO evaporation.

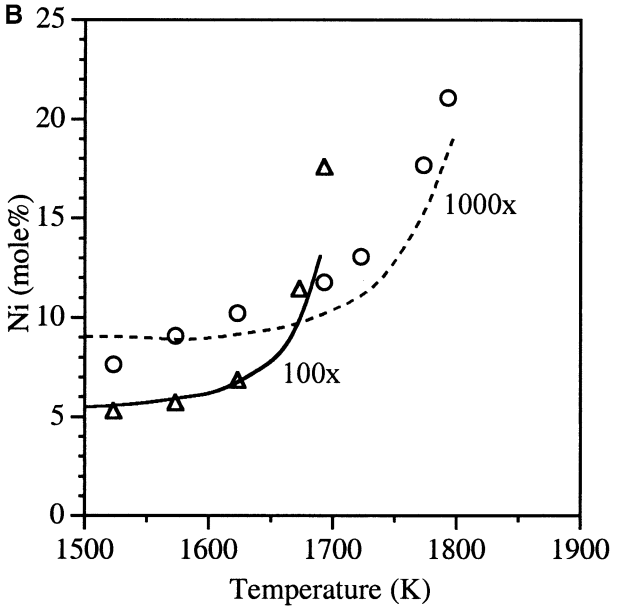

Fig. 1. (continued)

2.6. Scaling Rules

All calculations assume a uniform initial silicate melt diameter of 0.936 mm. No dust is present. Again this is to avoid introducing the size distribution of material as another free parameter. Because diffusion is not assumed to be important, the only results that are influenced by the choice of initial size are the times. All times scale with initial radius (t_r/t_{model} = r(mm)/0.468), making calculating times for different initial sizes straightforward.

Other simple scaling rules can be applied to the results. For instance, the "equilibrium" silicate melt compositions are largely determined by reactions of the form

$$MO_{(l)} + H_2 = M_{(g)} + H_2O, \quad \text{(R1)}$$

where M = Mg, SiO and Fe. At thermodynamic equilibrium, the activities of the oxide components in the melt are given by

$$a_{MO} = \frac{P_M P_{H_2O}}{P_{H_2}} e^{\Delta G/RT}. \quad (1)$$

In systems with CI solid enrichments of greater than ~3–4 times solar, the solid is the major O-bearing reservoir. On heating, the prime source of H_2O in the gas will be the water and O released from the solid. Consequently, the partial pressures of both M and H_2O are likely to be proportional to the absolute dust density (or dust enrichment times the total pressure). The partial pressure of H_2 is proportional to the total pressure minus the hydrogen consumed to make H_2O, so that at a given temperature

$$a_{MO} \approx \frac{ZD_g^2 P_{tot}^2}{P_{tot}(X - YD_g)} e^{\Delta G/RT}, \quad (2)$$

where D_g is the solid/gas/solar ratio, P_{tot} is the total pressure, and X, Y and Z are constants. For modest dust enrichments, the fraction of hydrogen consumed to make H_2O is small and Eqn. 2 reduces to

$$a_{MO} = D_g^2 P_{tot} K, \quad (3)$$

where K is a new constant. Eqn. 3 implies that there will be a range of conditions under which the same bulk "equilibrium" silicate composition exists. From Eqn. 3, the same "equilibrium" activities will occur at different total pressures but the same temperature when the ratio of the solid/gas/solar enrichments is given by

$$\frac{D_{g,i}}{D_{g,j}} = \sqrt{\frac{P_{tot,j}}{P_{tot,i}}}. \quad (4)$$

Using the "equilibrium" composition at $P_{tot} = 10^{-3}$ bars for a given temperature and solid/gas/solar ratio as a reference, the conditions under which the same composition is stable at the same temperature but lower P_{tot} can be estimated simply by dividing the solid/gas/solar ratio by $\sqrt{P_{tot}*1000}$. This approximation is least accurate, particularly for FeO, when temperatures and pressures are low and/or dust enrichments high. This is probably because there is competition for Fe between FeO and Fe-metal, and because of the consumption of H_2 to make H_2O.

The "equilibrium" compositions are achieved via evaporation, so the conditions required to produce a given maximum isotopic mass fractionation will scale in a similar way. Also, the evaporation rates for MgO, SiO_2 and FeO are proportional to $\sqrt{P_{H2}}$ (see EA1). Consequently, to a first approximation the ratio of the times required to reach these maximum isotopic fractionations and then equilibrate with the gas will scale in the same way as the ratio of solid/gas/solar enrichments in Eqn. 4.

Table 1. The initial solid and gas compositions (atomic). The solid composition is CI, but on heating the volatile component is assumed to immediately go into the gas.

	Silicate	Metal	Volatiles	Gas
H			5.39×10^6	2.79×10^{10}
He, etc.			2.73×10^9	
C			7.68×10^5	9.31×10^6
O	3.67×10^6		3.91×10^6	1.61×10^7
Na	5.73×10^4			
Mg	1.07×10^6			
Al	8.49×10^4			
Si	1.00×10^6			
S		5.15×10^5		
Cl			5.23×10^3	
K	3.76×10^3			
Ca	6.14×10^4			
Fe	3.79×10^5	5.21×10^5		
Ni		4.91×10^4		

3. RESULTS AND DISCUSSION

A total of ~1200 simulations under different conditions were run and the results are summarized and discussed below in three separate sections—(1) the "equilibrium" compositions, (2) the maximum isotopic mass fractionations (‰/amu) that develop, (3) the times it takes to reach the maximum isotopic fractionations and then to fall back to 0.25‰/amu. The latter time is somewhat arbitrary, but it is of the order of the isotopic

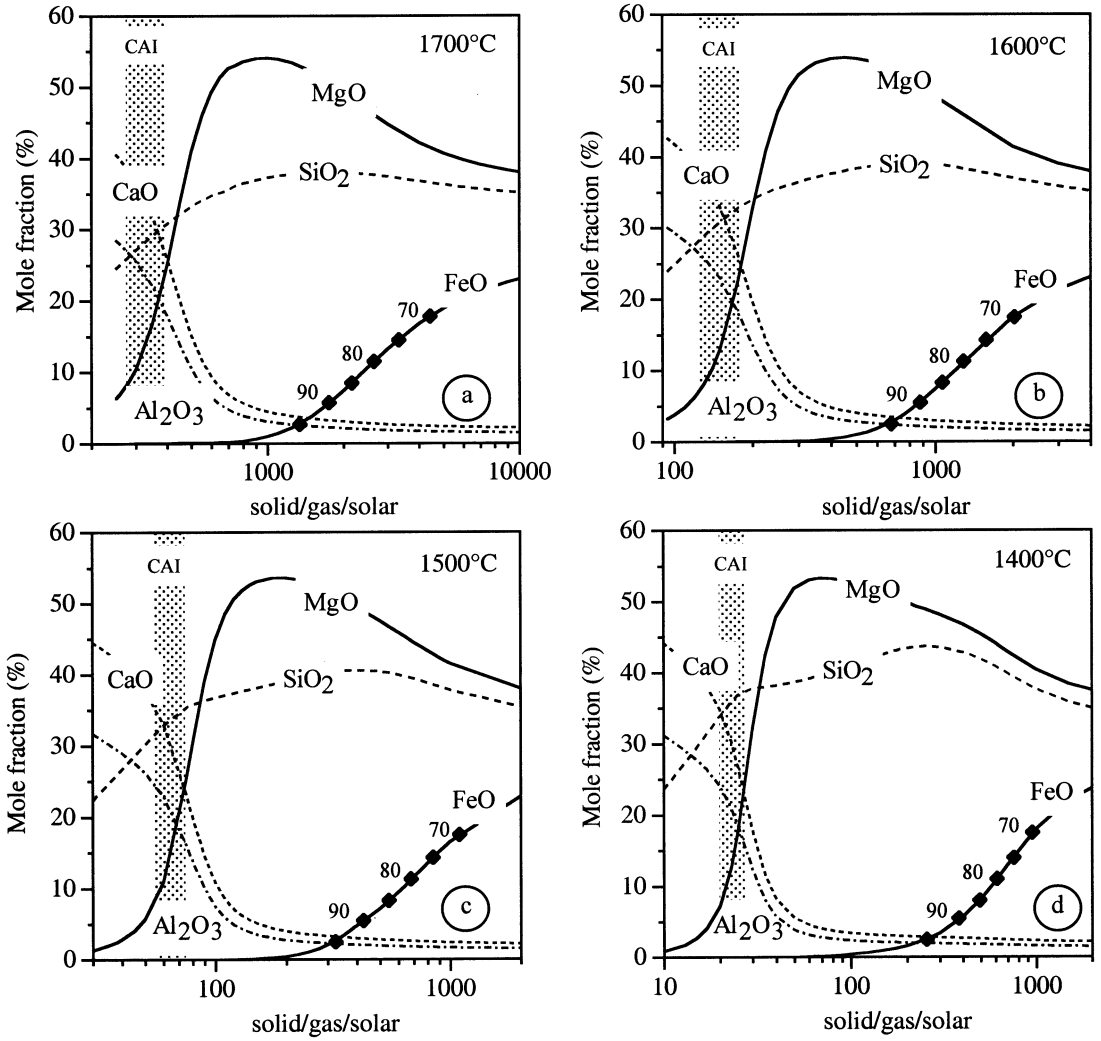

Fig. 2. The composition of "equilibrium" silicate melts as a function of initial solid/gas/solar ratio and temperature. The stippled region is the range of conditions where "equilibrium" melts with Type A and B CAI-like compositions form. The numbered symbols superimposed on the FeO abundance curve are the Mg#s (100 × Mg/(Mg + Fe) atomic) of the melts. The total pressure is 10^{-3} bars. To estimate the "equilibrium" compositions at lower pressures, divide the solid/gas/solar ratios by $\sqrt{P_{tot}*1000}$.

fractionations seen in chondrules and it gives an idea of the equilibration timescale.

3.1. "Equilibrium" Compositions

With their relatively modest isotopic mass fractionations, chondrules probably approached isotopic equilibrium with the gas. There is no experimental evidence that the alternative, multiple brief heating events (Wasson, 1993), is capable of producing chondrule textures. Calcium-aluminum-rich inclusions generally exhibit much larger isotopic mass fractionations. Nevertheless, their elemental compositions may have approached the equilibrium ones. Thus the "equilibrium" compositions are useful in trying to understand the conditions under which chondrules and CAIs formed. A number of previous studies have come to broadly similar conclusions about predicted equilibrium compositions. Here only some implications of these results are discussed.

The elemental compositions of the silicates are, to a reasonable first approximation, simple functions of D_g and P_{tot}. Hence in Figure 2, only the results for $P_{tot} = 10^{-3}$ bars are shown. To estimate the "equilibrium" compositions at lower pressures, divide the solid/gas/solar ratios in Figure 2 by $\sqrt{P_{tot}*1000}$. Also marked on Figure 2 are the range of conditions where "equilibrium" melts with Type A and B CAI-like compositions form, and the Mg#s (100 × Mg/(Mg + Fe) atomic) of FeO-bearing silicate melts.

As was found by Ebel and Grossman (2000), ferromagnesian silicates with Mg#s typical of chondrules form, at any given temperature, over a significantly higher and broader range of dust enrichments than more CAI-like compositions. The narrowness of the CAI-like region is largely determined by the

precipitous fall in the MgO contents at low dust enrichments, and could in part explain the difference in abundance between chondrules and CAIs.

The turbulent concentration mechanism is able to reproduce many aspects of chondrule and rim size distributions (Cuzzi et al., 2001; Cuzzi, 2004). Turbulent concentration predicts a spectrum of solid enrichments in the nebula that is dependent on the poorly constrained α value of the disk. The relative abundances of different chondrule types would be a function of the enrichment spectrum and ultimately may help constrain the α value of the disk. Given this predicted enrichment spectrum, some CAI-like objects should be made in regions of low solid enrichment during chondrule formation. Their presence or absence would be a test of the turbulent concentration mechanism. Perhaps this is the explanation for some of the CAIs that have relatively low short-lived radionuclide contents (MacPherson et al., 1995), and even compound objects like that described by Itoh and Yurimoto (2003). Whether the O isotope systematics of these CAIs can be explained by formation in the chondrule forming region will depend on the origin of the mass independent fractionations. The apparent absence of chondrules with "canonical" radionuclide abundances points to disk conditions at the time and place where radionuclide-rich CAIs formed that prevented solid enrichments of 100s-1000s solid/gas/solar developing.

Figure 2 suggests that the range of chondrule and CAI silicate compositions can be explained by their having formed over a range of temperatures and/or dust enrichments. That such a wide range of compositions can, in principle, be produced at the same temperature simply by changing the initial solid/gas ratio provides a cautionary note. Evaporation of FeO and silica from a melt will increase its liquidus temperature (Delaney, 1995; Alexander, 1996; Cohen et al., 2003). Not only will the loss of FeO and silica cause a melt to become undercooled, influencing the texture that develops, but the liquidus temperature of the final bulk composition would provide an overestimate of the peak temperature achieved during formation. Thus if chondrules had CI-like precursors, it is likely that many of them never achieved the liquidus temperatures of their present compositions, although their textures suggest that they were largely or entirely molten when they formed.

While in general the results in Figure 2 appear to explain the range of chondrule and CAI compositions, in detail there are significant deviations of some chondrule/CAI compositions from the predicted ones. Indeed, a perfect match between calculated and natural chondrules/CAIs would not be expected given the uncertainties in the thermodynamic models and in the formation conditions (P, T, precursor compositions, etc.). Figure 3 compares the Mg, Si and Al contents of several classes of object with the predicted bulk compositions of the "equilibrium" melts.

Type A chondrules, and Type A and B CAIs, are broadly consistent with the predictions (Figs. 3a,b). There is some scatter in the data. In part, this may simply be because the compositions were determined on 2-D sections that are not representative of the bulk chondrule or CAI. Even if the section is representative, it can be difficult to determine the bulk composition accurately because a large number of analyses must be made and density differences between phases need to be taken into account.

Grossman et al. (2000) suggested that the reason for the large scatter in the Ca/Al ratios of Type A and B CAIs is due to nonrepresentative analyses, principally of spinel. There is a group of Type B CAIs in Figure 3a that form a trend towards higher MgO and Al_2O_3 contents along a slope of $\sim$1, consistent with the addition of spinel. In chondrules, there is much less scatter in Ca/Al ratios, probably because in chondrules both Ca and Al are primarily in the glass.

Unrepresentative analyses may also account for some of the more silica-rich compositions of type B chondrules, Al-rich chondrules and type C CAIs (Figs. 3c,d). Type B chondrules are usually identified on the basis of the abundance of pyroxene in them. This may bias selection of chondrules for sections that are the most pyroxene-rich and therefore have more silica-rich compositions than in bulk. Aluminum-rich chondrules are most easily found if they are plagioclase- or glass-rich, and there will be a bias towards finding sections that are richer in these phases. However, it is unlikely that selection biases and unrepresentative analyses can explain all of the silica-rich and Al-rich chondrule data. Whether there are any biases involved in the identification and analysis of POIs and Type C CAIs is unclear.

The compositions of the more silica-rich objects in Figures 3c,d could be explained by a silica enrichment in the regions where they formed. However, these enrichments would have to be large. Figures 3c,d include curves for a bulk composition that has twice the CI silica content. The type B chondrules and some of the Al-rich chondrules could be explained by this level of silica enrichment, but most Al-rich chondrules and all Type C CAIs would require even greater enrichments. While it cannot be ruled out, it is difficult to envision how relatively large regions of the nebula could have developed bulk compositions that were significantly more silica-rich than CI.

Is there another explanation? There is a temperature dependence to the "equilibrium" MgO and silica contents, but it would require equilibration temperatures of less than 1400°C to reproduce the silica-rich compositions of these chondrules and CAIs, which seems unlikely. One possible explanation for these more silica-rich objects is that the curves are for the bulk "equilibrium" compositions. Even if the material in a chondrule/CAI formation region as a whole is at equilibrium, individual chondrules/CAIs in that region need not have the same bulk compositions. All that is required is that their constituent components (minerals and melt) have the equilibrium compositions. Variations in bulk composition would mostly reflect the diversity in the compositions of the precursors. For example, if a chondrule precursor is Mg-rich compared to the average, rather than lose Mg by evaporation the chondrule might crystallize more olivine than on average. Thus, some diversity in the bulk compositions of individual chondrules/CAIs is possible even when they equilibrated together in the same event.

There will also be instances when the compositions of their precursors prevent chondrules/CAIs from reaching equilibrium. For example, precursors may have had a range of Ca/Al ratios. Differences in the absolute and relative abundances of Ca and Al will influence the activities of other components. However, chondrules, and possibly many CAIs, would be unable to change their Ca/Al ratios because Ca and Al evaporation rates are too slow. Instead, the compositions of the melts would evolve via evaporation/condensation and/or crystalliza-

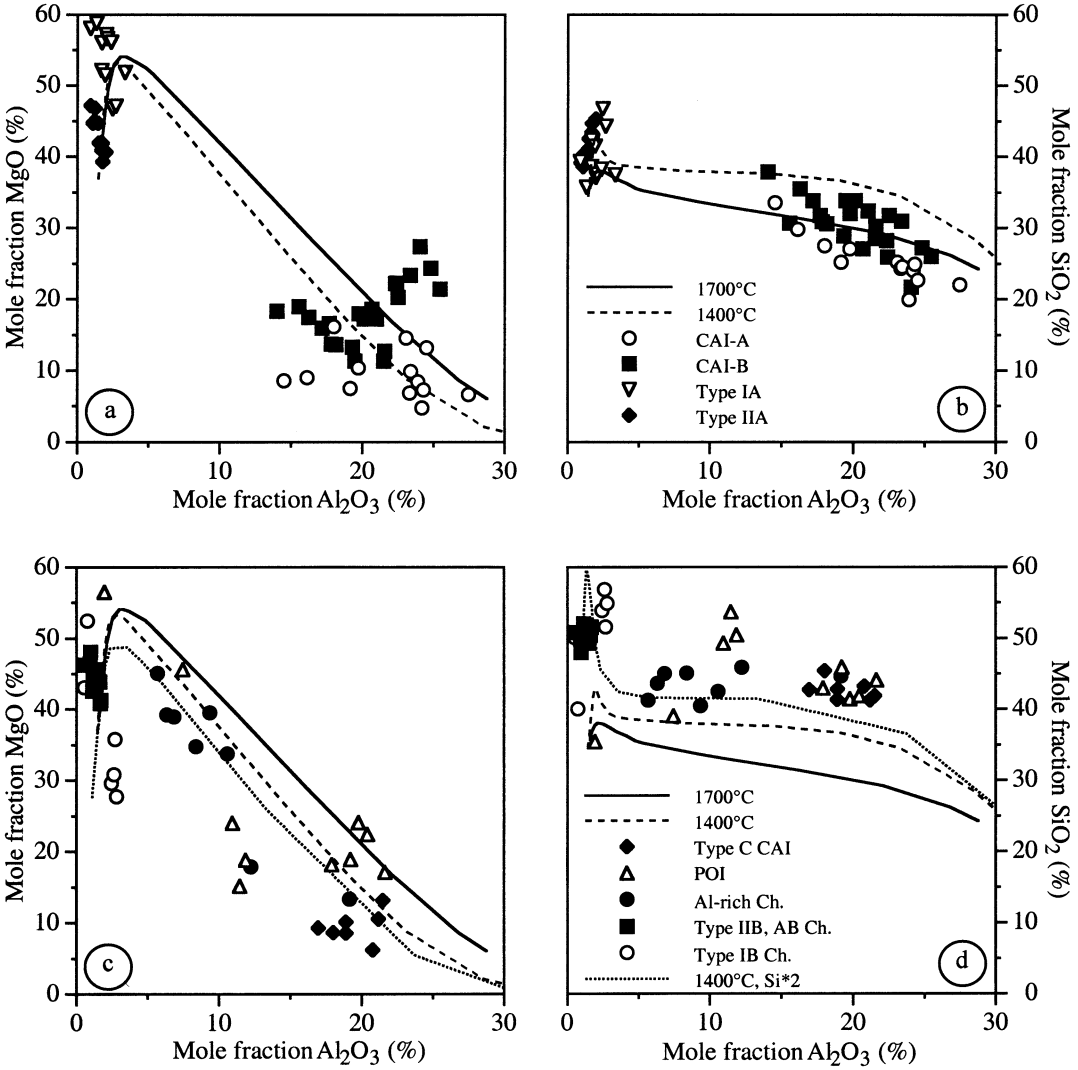

Fig. 3. Comparison of the "equilibrium" silicate melt compositions with those of chondrules and inclusions (Bischoff and Keil, 1984; Beckett, 1986; Wark, 1987; Jones and Scott, 1989; Jones, 1990, 1994, 1996; Sheng et al., 1991). Only Al-rich chondrules with low FeO and Na_2O contents are plotted on the assumption that these are the least altered ones. Type A chondrules and, Type A and B CAIs (a, b) roughly conform to the predictions. On the other hand, type B and Al-rich chondrules, POIs and Type C CAIs (c, d) are systematically more silica-rich than the "equilibrium" melts. Also shown in (c, d) are curves for a bulk composition that has twice the silica content of CI.

tion to minimize their chemical potentials relative to the gas. There may be other situations where crystal and melt compositions are not the equilibrium ones, but the difference in chemical potentials (the driving force for equilibration) between them and the equilibrium compositions are small enough that equilibration does not occur over chondrule/CAI formation timescales. The range of compositions that are possible in any one formation event will probably need to be determined numerically.

Thus, it is possible that some chondrules/CAIs were on average more silica-rich than the bulk provided that other more silica-poor objects also formed. If this is the explanation of the type B chondrules, Al-rich chondrules and Type C CAIs, there must be a class of silica-poor objects to counterbalance them. However, there are no abundant classes of chondrule or CAI with the requisite complimentary compositions.

The one possible counterbalance that could either be overlooked in meteorites or be fractionated from chondrules/CAIs in the nebula is dust. Not only will dust evaporate more rapidly than chondrules and CAIs at the same temperature, but under some circumstances it is heated to higher temperatures than the larger chondrules/CAIs (Desch and Connolly, 2002). If, for example, the dust were hotter than the chondrules and became forsterite-rich through rapid evaporation of FeO and silica, some of this silica would condense on the cooler chondrules/CAIs making them more silica-rich than the bulk solid composition. If the heating was more intense and/or solid/gas/solar enrichments were modest, partial evaporation of refractory elements from the dust and recondensation of them onto the cooler larger objects could explain Group II-like REE patterns in molten CAIs. If molten CAIs with Group II patterns formed in this way, their isotopic compositions are likely to be less

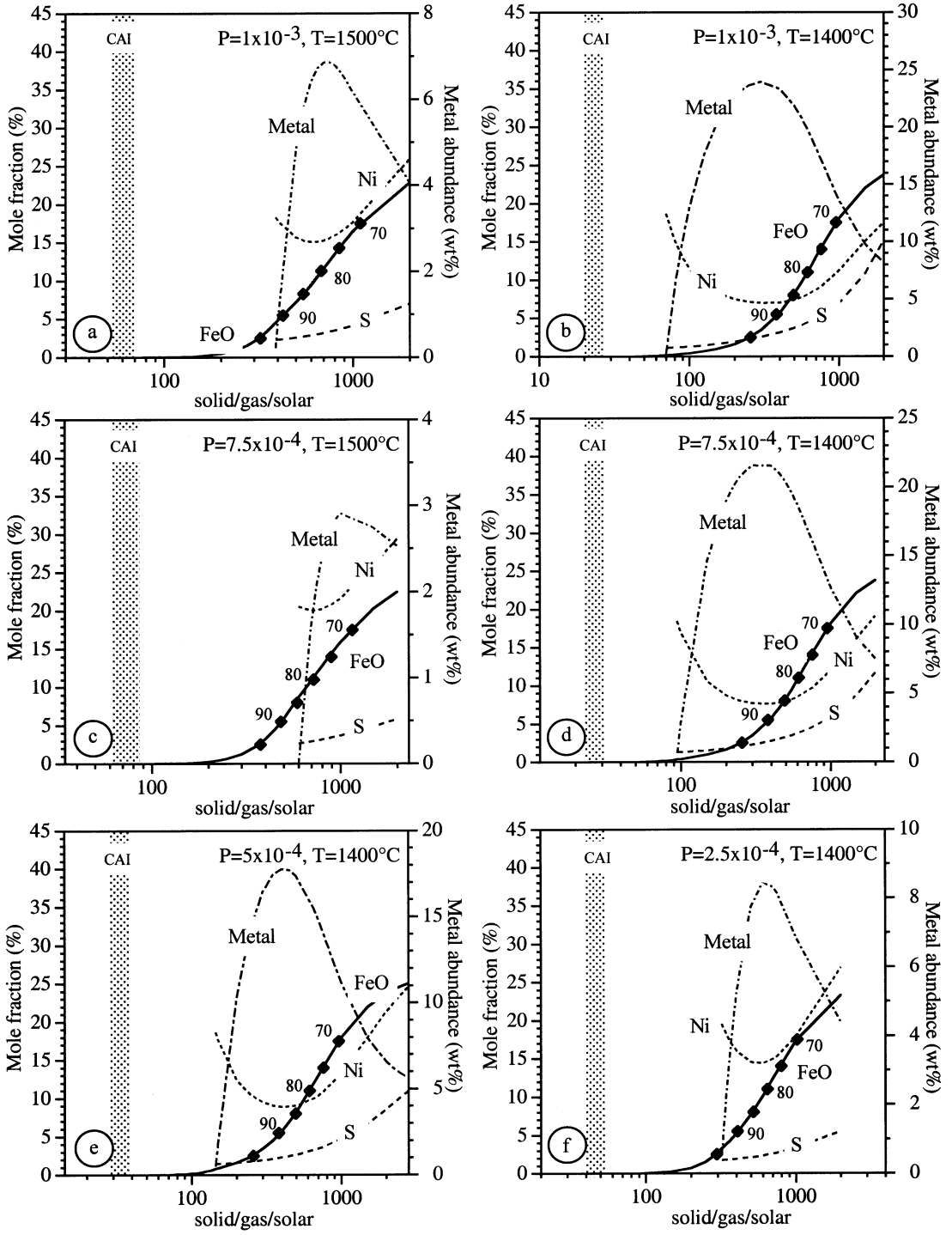

Fig. 4. The predicted "equilibrium" Fe-Ni-S melt abundances (wt %) and, the Ni and S contents (mole %) in the metal melt for various conditions. Also shown for reference is the region where CAI-like silicate compositions would form (stippled), and the equilibrium FeO content (solid line) and the Mg# (filled triangles) of the silicate melts.

fractionated than other molten CAIs. Again such scenarios will have to be tested numerically.

The abundance and composition of metal is often overlooked or only discussed briefly when comparing chondrules with calculated equilibrium compositions. Figure 4 shows the metal composition and abundance, relative to silicates, as a function of dust enrichment, along with the bulk FeO content and the Mg# of the silicate material. The metal composition does not scale as simply as the silicate compositions with total pressure, partly because its equilibrium composition is not a direct function of P_{H2}, so the results for a number of total pressures where metal is stable are shown.

Metal is not stable at 1600°C or above under any of the conditions that were explored. Many chondrules have liquidus temperatures of 1600°C or above, although they may not have reached them when they formed. However, if metal-bearing chondrules did reach temperatures of 1600°C or above, either they formed under different conditions to those assumed here or interior metal was slow to equilibrate with the gas.

Ebel and Grossman (2000) pointed out that metal is subject to oxidation at high dust enrichments and evaporation at low dust enrichments. The range of solid/gas ratios over which metal is stable increases with decreasing temperature at constant total pressure, but decreases with decreasing total pressure. The influence of evaporation and oxidation can also be seen in the U-shaped Ni abundance curves. At $P_{tot} = 10^{-3}$ bars, the peak in the predicted metal abundance occurs at a Mg# of ~78 at T = 1500°C, and at a Mg# of ~93 at 1400°C. At 1500°C and lower pressures, the region of metal stability shrinks dramatically, and has all but disappeared at 2.5×10^{-4} bars. At 1400°C, the region of metal stability has disappeared by10^{-4} bars.

There have been no systematic studies of metal abundance as a function of chondrule type. However, typically metal abundances are lower in type IIs (Mg# $\leq$ 90) than in type Is, and the Ni contents of metal in many very FeO-poor type Is are also lower than in other chondrules (Rambaldi and Wasson, 1981; Scott and Taylor, 1983; Rambaldi and Wasson, 1984). Both these observations seem to be inconsistent with the predictions of the model. In Figure 4, the peak in the metal abundance for several conditions occurs in the type II chondrule field. At 1500°C and total pressures for which there is a region of metal stability, many type I chondrules are predicted to have little or no metal at all. Type II chondrules, even those with Mg# $\leq$ 70, are predicted to have significant metal contents under all conditions when there is a region of metal stability. Finally, under almost all conditions, the metal in the most FeO-poor type I chondrules is not predicted to be the most Ni-poor.

All of these predictions are contrary to what is seen in CR chondrites, for instance. In CR chondrites, most chondrules are type I (Mg# = 99–95) and contain abundant metal with typical Ni contents of ~4–7 mol% (Connolly et al., 2001). It is always difficult to know how representative of the bulk metal composition analyses are. The over or under representation of taenite in the analyses can change the estimated bulk composition considerably. Nevertheless, there do seem to be significant differences between model predictions and what is seen in chondrules.

Some of the inconsistencies in the observed and predicted metal abundances could simply reflect the efficiency of metal expulsion from different types of chondrule. The low Ni content of metal in some type I chondrules and the high predicted abundance of metal in type IIs are more difficult to explain. The predicted abundance of metal shifts to higher Mg# with increasing total pressure, and the Ni content of metal at a given Mg# decreases. It is likely that when $P_{tot} > 10^{-3}$ bars, the bulk metal content will peak when the Mg# > 90. However, astrophysical models suggest that $P_{tot} \approx 10^{-3}$ bars is a likely upper limit for chondrule formation.

Type II chondrules with no metal could be produced if they formed at high dust enrichments and T > 1500°C, i.e., at higher temperatures than metal-bearing type Is. Blander et al. (2001) have suggested that if metal completely evaporates on heating, then on cooling its nucleation and condensation might be suppressed, "forcing" Fe to condense as FeO in the silicate melt. If correct, type II chondrules could form at similar dust enrichments to type Is, but experienced higher peak temperatures. However, generally the formation temperatures of type IIs are thought to be less than for type Is. Type IIs could have formed at lower total pressures than considered here and high dust enrichments when metal would not be stable but, as will be discussed later, in this case timescales for equilibration may become too long. Finally, type IIs may have formed after significant metal-silicate fractionation, but this explanation is difficult to test.

A common explanation for low-Ni metal in type I chondrules is reduction of FeO, most likely by C (Kracher et al., 1983; Connolly et al., 1994; Zanda et al., 1994). If all chondrules that formed in a single event approached equilibrium with one another, this means that most or all chondrules that formed in a reducing event must have had precursors that were more reduced (less volatile O and/or more C) than CI.

Alexander (2002b) suggested that primordial dust was similar to cluster IDPs, which are anhydrous, C-rich and FeO-poor. Even very modest enrichments of dust of this composition produce very reducing conditions (Ebel and Alexander, 2002). To produce more oxidizing conditions requires that ice is concentrated along with the dust. The ratio of ice/(silicate+metal+sulfide) would be a function of the ambient temperature and the total pressure. Any variations in these two parameters would ultimately influence the Mg# and metal abundance that develop in chondrules. Therefore, the ambient temperature and pressure may have been as important as the solid enrichment and formation temperature in determining chondrule compositions. Also, if there was recycling of material during repeated heating events, the tendency would be for chondrules to become more oxidizing as the fraction of C-rich primordial dust decreases.

It should be emphasized that metal abundances could vary considerably from chondrule to chondrule, even if they formed and equilibrated in the same event. The metal must have the same composition in all chondrules that were at equilibrium with one another, but metal abundances will depend on precursor compositions and how efficiently metal is expelled from the chondrules.

Finally, the model predicts that there will be modest abundances of S in the metal melt, even in type I chondrules, and that the S content should increase with decreasing Mg#. This is broadly consistent with what is seen in chondrules from the lowest petrologic type OCs (Hewins et al., 1997; Rubin et al., 1999). However, the results reported here should be treated with caution since crystallization is not taken into account. Ebel and Grossman (2000) find at $P_{tot} = 10^{-3}$ bars and solid/gas/solar = 1000 that the first S-bearing phase to condense is pyrrhotite at ~1100°C, but they did not include a Fe-Ni-S melt in their calculations. Also, small amounts of S (up to ~0.2 mol%) are soluble in Fe-Ni-alloys at high temperatures (Chuang et al., 1985). Both this study and Ebel and Grossman (2000) demonstrate that in dust enriched systems S cannot always be considered as a volatile element. This may go some way to explaining the enrichment of S in ordinary chondrites relative to elements that are normally assumed to have similar

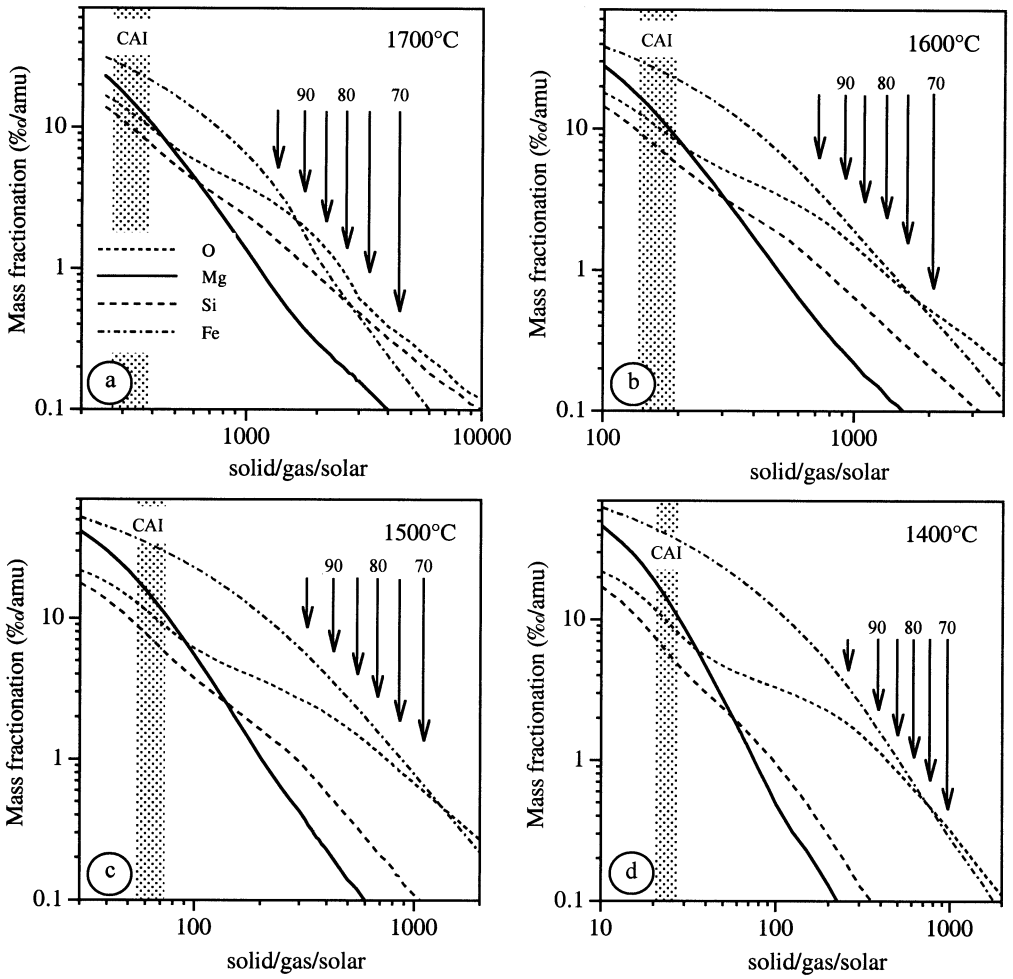

Fig. 5. The maximum isotopic mass fractions of O, Mg, Si and Fe that develop in the silicate melts as a function of initial solid/gas/solar ratio and temperature. The numbered arrows indicate the equilibrium Mg#s of the melts at these solid/gas/solar ratios. The total pressure is 10^{-3} bars. To estimate the mass fractionation at lower pressures, divide the solid/gas/solar ratios in by $\sqrt{P_{tot}*1000}$.

volatilities based on equilibrium calculations at $P_{tot} = 10^{-4}$ bars and no dust enrichment (Palme et al., 1988). Combining the Mg# and the metal composition of chondrules may ultimately prove to be a useful means of constraining the conditions of chondrule formation.

3.2. Isotopic Fractionation

Producing the "equilibrium" silicate compositions always involves some evaporation because the equilibrium gas must be generated. Positive isotopic mass fractionation will be associated with this evaporation. For "equilibrium" silicate compositions with Mg#s < 74, there will also be some net condensation because their FeO contents are higher than the initial FeO content (Table 1). Most of this FeO comes from evaporation and oxidation of metal. As a result, the Fe isotopic evolution in these silicates is more complex, with in some cases negative mass fractions of ~2–3‰/amu developing before final equilibration. Figure 5 only shows the maximum positive isotopic mass fractionations that develop in the PCR model when $P_{tot} = 10^{-3}$ bars. The maximum fractionations that develop in the EQR model are similar and are not shown. As with the elemental compositions, to estimate the conditions for producing the maximum fractionations at lower pressures, simply divide the solid/gas/solar ratios in Figure 5 by $\sqrt{P_{tot}*1000}$.

The maximum fractionations are a function of the solid/gas/solar ratio and are correlated with the "equilibrium" elemental compositions—the more evaporation needed to achieve the "equilibrium" composition, the greater the mass fractionation. As will be discussed in more detail in the next section, they also develop on timescales that are shorter than or comparable to estimates of chondrule and CAI formation. Because of gas-melt exchange, the maximum isotopic mass fractionations that develop are not as large as would be predicted by Rayleigh fractionation (Fig. 6). If chondrules and CAIs formed at similar or higher total pressures and dust enrichments to those considered here, the use of Rayleigh fractionation calculations to estimate the amount of an element that was lost would be very misleading.

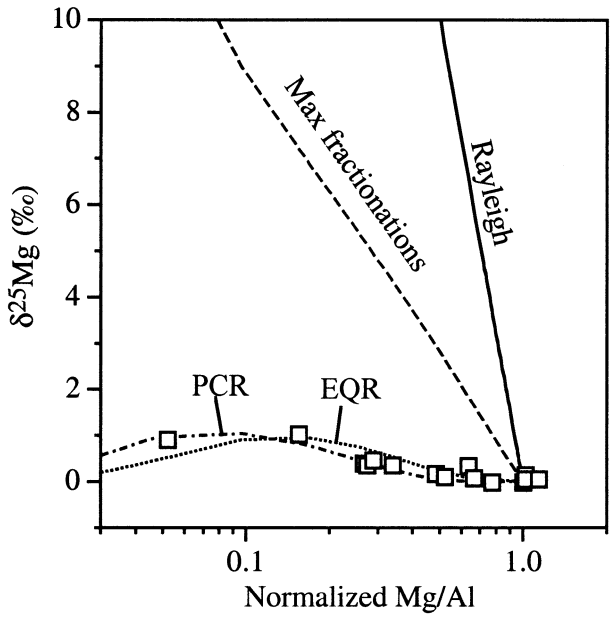

Fig. 6. The Mg isotopic compositions and normalized Mg/Al ratios of some Allende chondrules (Galy et al., 2000). These are compared to the compositions produced by Rayleigh fractionation, the maximum isotopic fractionations in model chondrules formed at various solid/gas/solar ratios (>60), and the model chondrule compositions after 270 min in the PCR model and 470 min in the EQR model. Other assumed conditions for the modeling were 1500°C and $P_{tot} = 10^{-3}$ bars.

3.2.1. Chondrules

The maximum fractionations that develop when forming chondrule-like compositions are generally larger than have been seen in recent high precision studies. This either requires very different conditions to the ones assumed here, or formation times that are long enough to allow gas and melt to approach equilibrium.

Galy et al. (2000) report modest Mg isotope mass fractionations in Allende chondrules (Fig. 6) that are an inverse function of the Mg/Al ratio. An inverse relationship between Mg isotopic composition and Mg/Al ratio is expected if evaporation was responsible for the elemental fractionations. However, the isotopic fractionations are much smaller than predicted by Rayleigh fractionation and even than the maximum values calculated by the models (Figs. 5 and 6). Galy et al. (2000) suggest that this was because chondrules formed at total pressures of near one bar, when isotopic fractionations would be much less than predicted by Rayleigh fractionation. However, as discussed above, such high pressures seem astrophysically implausible.

If the chondrules studied by Galy et al. formed under the conditions considered here from a CI-like starting material, at some stage they will develop maximum mass fractionations similar to the maximum mass fractionations shown in Figure 6. The much more subdued Mg isotopic fractionations seen in the chondrules mean that there must have been considerable re-equilibration between chondrules and gas.

To illustrate the effects of reequilibration, PCR and EQR simulations were carried out in which chondrules were heated to 1500°C at $P_{tot} = 10^{-3}$ bars and a range of solid/gas/solar enrichments (≥60) for a constant length of time (Fig. 6). The times, 270 min in the PCR model and 470 min in the EQR model, were chosen to roughly fit the Galy et al. (2000) chondrule data and are consistent with estimates of chondrule formation timescales. The resulting curves from these simple simulations reproduce the chondrule compositions very well. The chondrules are unlikely to have experienced such simple thermal histories. Nevertheless, the results show that the Galy et al. explanation for them is not required. Indeed, the conditions and timescales necessary for reequilibration to reproduce the chondrule compositions are consistent with a canonical nebula.

If reequilibration is the explanation for the chondrule compositions, their thermal histories would have to have given them sufficient time to equilibrate with the gas at high temperatures, but during cooling little or no further equilibration can have occurred. If equilibration continued to low temperatures, all the chondrules would have similar elemental and isotopic compositions. Closure of chondrules to exchange at lower temperatures was probably greatly aided by crystallization, slow diffusion rates in the SiO_2-rich residual melts, and condensation on the fine dust that formed chondrule rims and interchondrule matrix. Thus, exploring the sort of more realistic thermal histories that would be needed to reproduce the Galy et al. data are beyond the scope of this paper.

3.2.2. Calcium-Aluminum-Rich Inclusions

The correlated fractionations observed in Mg, Si and O (Figs. 7 and 8) have been a longstanding problem for explanations of CAI formation. The correlations are not what is observed from evaporation experiments. Estimates of how much Si and Mg were lost, assuming Rayleigh fractionation, indicate nonsolar precursors. Recent attempts to explain the CAI compositions involve a two stage process (Grossman et al., 2000; Richter et al., 2002). The first step is the formation of the precursors of CAIs by equilibrium condensation. It is during the subsequent melting stage that evaporation and isotopic fractionation occur.

The motivation behind the two stage model is the apparent nonsolar composition of CAI precursors estimated from the isotopic compositions of CAIs assuming Rayleigh fractionation. However, as was pointed out earlier, the fractionations that develop under the conditions assumed here are less than predicted by Rayleigh fractionation. Indeed, the predicted maximum fractionations for CAIs are similar to those observed.

In Figures 7a,b and 8a,b, the isotopic evolutionary paths of objects that develop CAI-like elemental compositions in the PCR and EQR models, respectively, are compared with the CAI data. At $P_{tot} = 10^{-3}$ bars, CAI-like equilibrium elemental compositions form between $D_g \approx 60-80$ at 1500°C and between $D_g \approx 20-30$ at 1400°C (Fig. 2). At constant temperature and $D_g\sqrt{P_{tot}*1000}$, the evolutionary paths are very similar for different total pressures. The time it takes to evolve along these paths will vary with $1/\sqrt{P_{tot}*1000}$.

In Figures 7 and 8, during the initial evaporation phase (loss of alkalis, FeO and SiO_2) Si and O isotopic fractionations develop more rapidly than for Mg. This is similar to what is observed in evaporation experiments (Wang et al., 2001), and

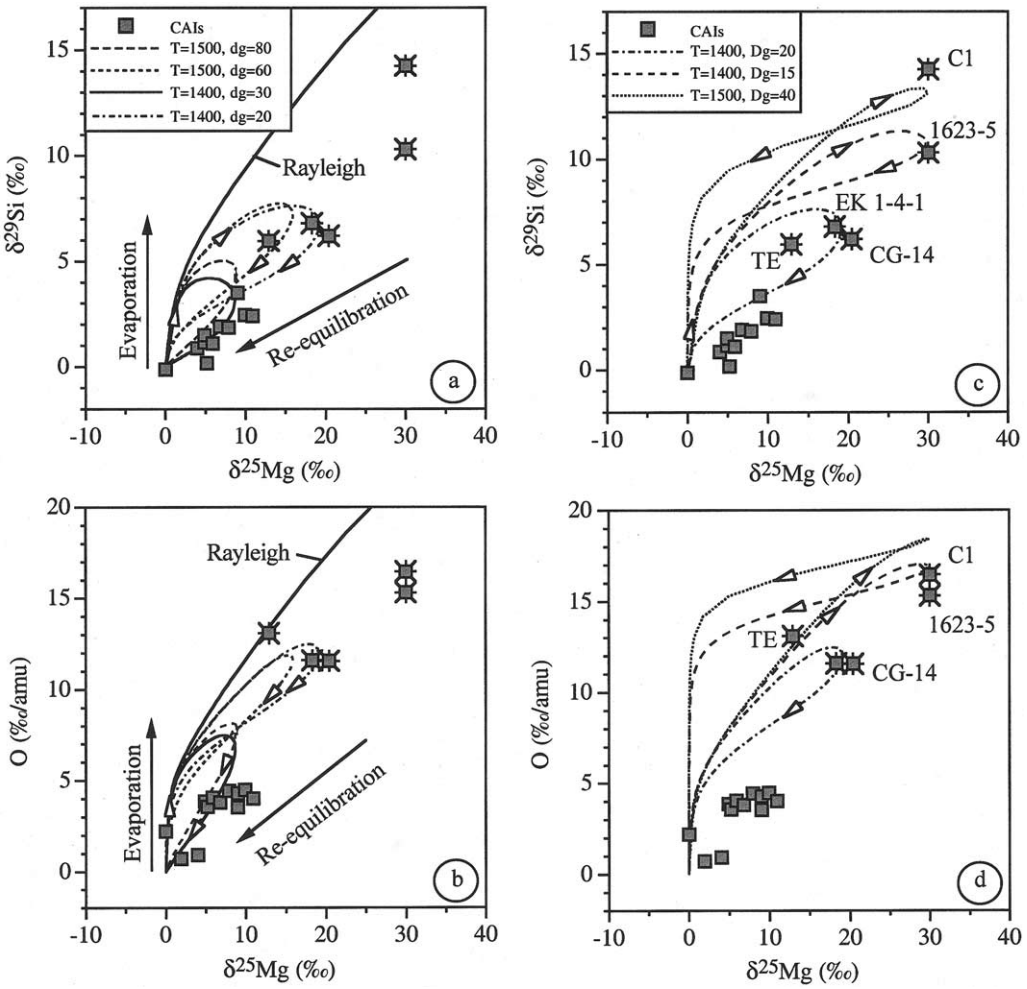

Fig. 7. Comparison of bulk CAI isotopic compositions with PCR model evolution paths under various conditions. The CAI data are from Clayton et al. (1987, 1988), but with all inclusions with negative Si mass fractionation excluded (Grossman et al., 2000). The O isotopic mass fractionations in the CAIs were estimated assuming that all CAIs evolved from a slope one line that passes through the origin in an O three isotope diagram. The starred symbols are for FUN or FUN-like inclusions. All the simulations assume a total pressure of 10^{-3} bars, but simulations at lower pressures with the solid/gas/solar ratios divided by $\sqrt{P_{tot}*1000}$ produce very similar results. In (a, b) the simulations assume solid/gas/solar ratios at the lower and upper bounds for producing CAI-like "equilibrium" melt compositions at 1400°C and 1500°C (Fig. 2). Also shown in these figures are curves for evaporation of a CI-like melt under Rayleigh conditions. In (c, d), the solid/gas/solar ratios assumed in the simulations are at or below the lower bound for producing "equilibrium" CAI-like melt compositions.

contrary to what is observed in CAIs. As evaporation proceeds, gas pressures build up and, because of changes in the component activities in the melt, Mg becomes more volatile. The resulting increases in both the isotopic fractionation of Mg and the rate of reequilibration of Si and O with the gas causes the compositions to evolve towards the right of the diagram and the Rayleigh line. Eventually, reequilibration becomes the dominant process and the compositions evolve back towards the origin. The relative rates of reequilibration of Mg and Si under these conditions cause the paths to evolve along trajectories that more or less coincide with the trends seen in non-FUN CAIs. At temperatures of 1600°C and above, the curves fall above the CAI compositions. Thus, solid enrichments near the upper limit for CAI-like equilibrium compositions and temperatures of 1500°C or less best reproduce the non-FUN CAI data. At present, too many uncertainties remain for a more quantitative statement about non-FUN CAI formation conditions to be justified—accurate α coefficients need to be determined for the entire range of temperatures and P_{H2}, and the influence of crystallization will have to be explored.

Replication of the non-FUN O isotope data (Figs. 7b and 8b) is somewhat less successful than for the Mg and Si isotopes (Figs. 7a and 8a). Most, but not all, points lie below and to the right of even the higher solid enrichment curves. A number of factors might have contributed to this. There is some uncertainty in the O isotopic mass fractionations in the CAIs. They were estimated on the assumption that the CAIs evolved off a slope 1 line that passed through the origin in an O three isotope diagram. If CAIs started off on a line that had a different position and/or a different slope, this would alter the mass

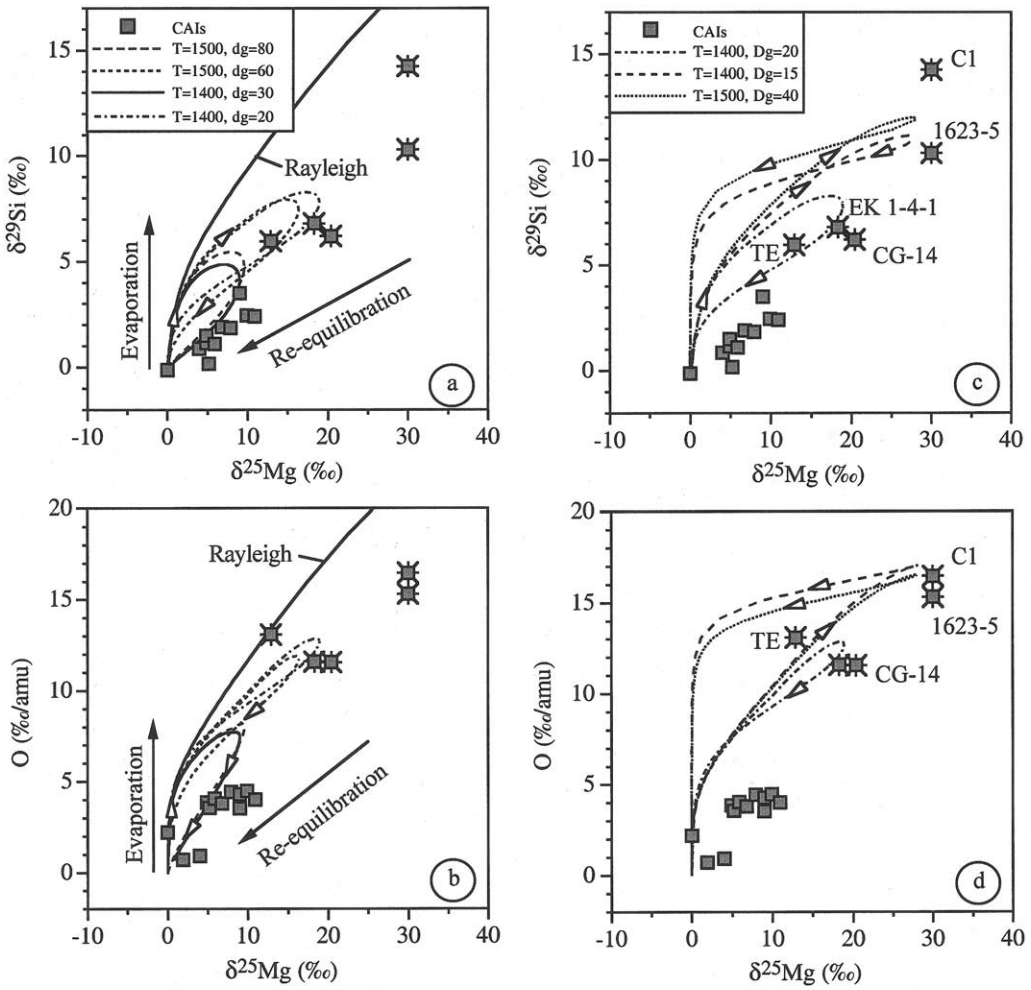

Fig. 8. Comparison of bulk CAI isotopic compositions with EQR model evolution paths under various conditions. The starred symbols are for FUN or FUN-like inclusions. See Figure 7 for more details about the sources of the CAI data and conditions assumed in the simulations.

fractionation estimates. In addition, most of the CAIs are from Allende and some part of their bulk O mass fractionation may be the result of later alteration (Young and Russell, 1998). The O mass fractionations will have been overestimated in the calculations if the precursors were less FeO-rich than assumed (see section 2.5). Lastly, it is also possible that direct gas-melt exchange, which is not considered here, caused O isotopic equilibration to be faster than predicted by the model.

The range of conditions over which the isotopic reequilibration trajectories coincide with those of the non-FUN CAIs is quite limited. Intriguingly, they are also the conditions needed to produce CAI-like equilibrium elemental compositions (Fig. 2), and Type B CAI mineralogies and textures (Stolper, 1982; MacPherson et al., 1984; Stolper and Paque, 1986), although these results will need to be confirmed with calculations that include realistic treatments of crystal growth, etc. At 1600°C and above, all curves fall to the left of the non-FUN CAIs. The curves best fit the CAI compositions during the reequilibration phase. At present, it cannot be ruled out that some of the initial evaporation could take place at temperatures significantly above 1500°C, but it seems likely that most of the equilibration would have to take place at 1500°C or below. If the solid/gas/solar ratios drop below the range where CAI-like compositions would form, the paths also fall above the non-FUN inclusions (Figs. 7c,d and 8c,d).

The FUN inclusion isotopic compositions are consistent with their having formed at or below the lower edge of the CAI solid/gas/solar ranges (Figs. 7c,d and 8c,d). It is possible that the FUN inclusions formed over a broader range of temperatures than the non-FUN inclusions. However, this cannot be tested here because at temperatures of ≥1600°C and the conditions needed to try to reproduce inclusions C1 and 1623-5 in particular, the melt develops compositions where the evaporation and/or activity coefficients become rather uncertain (see EA2). The FUN inclusion compositions also suggest that they have experienced less reequilibration with the gas than the non-FUN CAIs. Perhaps this explains why the FUN inclusions still retain some nuclear anomalies (the UN in FUN).

The bulk elemental composition of a CAI gives a good estimate of the $D_g\sqrt{P_{tot}*1000}$ for a given temperature. The isotopes and petrology suggest formation temperatures of

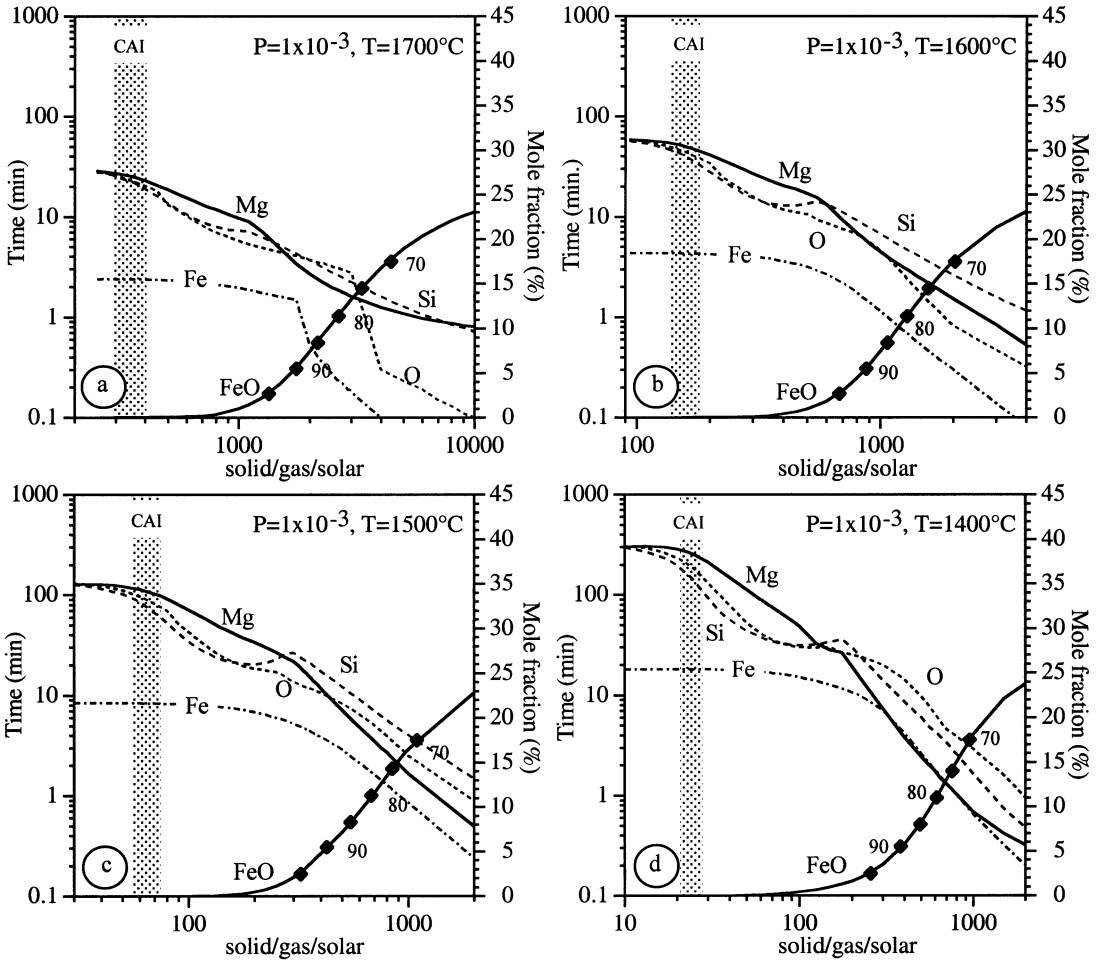

Fig. 9. The times (minutes) required in the PCR model to reach the maximum isotopic mass fractionations of O, Mg, Si and Fe in the silicate melts when $P_{tot} = 10^{-3}$ bars. To estimate times at lower for P_{tot}, divide both the times and solid/gas/solar ratios by $\sqrt{P_{tot}*1000}$. Also shown for reference is the region where CAI-like silicate compositions would form, and the FeO content (mole %) and the Mg# of the silicate melts.

~1400 to 1500°C. The modeling cannot be used to place limits on the total pressure without some knowledge of the timescales for CAI formation. Those timescales will have to be shorter than the equilibration timescales.

3.3. Timescales

The times required to produce significant isotopic fractionation (Figs. 9 and 10) and subsequent reequilibration with the gas (Figs. 11 and 12) provide useful constraints for both chondrule and CAI formation. Figures 9 and 10 only show the results for $P_{tot} = 10^{-3}$ bars. To estimate times at lower pressures divide the times and solid/gas/solar ratios by $\sqrt{P_{tot}*1000}$. The initial radius of the silicate melt was 0.468 mm. Times for objects with different initial sizes can be estimated by multiplying the times by r(mm)/0.468. To a first approximation, the isotopic composition of a melt increases linearly with time to the maximum mass fractionation and then decays exponentially towards the bulk composition, although obviously there is significant curvature as the melt approaches the peak mass fractionation.

Despite being calibrated against the same set of experiments, the timescales for evaporation and reequilibration predicted by the EQR model are generally about twice those for the PCR model. This is because the ratio of the maximum rates predicted by the two models vary with the conditions and the models have only been calibrated under a very limited set of conditions. Also, unlike in the experiments, in the solid enriched conditions assumed here the partial pressure of H_2O in particular in the nebula gas is high relative to the equilibrium partial pressure over the melts. Until equilibrium is reached, the two models treat the influence of the gas composition on the evaporation/condensation rates rather differently.

Not included in Figures 9 and 10 are the times at which significant negative Fe isotope mass fractionation develops in silicates, particularly those with Mg# < 0.74. These negative mass fractionations are associated with the net transfer, via evaporation and recondensation, of Fe from metal. This process is the cause of the complex behavior seen in the isotopic equilibration times of Fe at high solid/gas/solar ratios (Figs. 11 and 12).

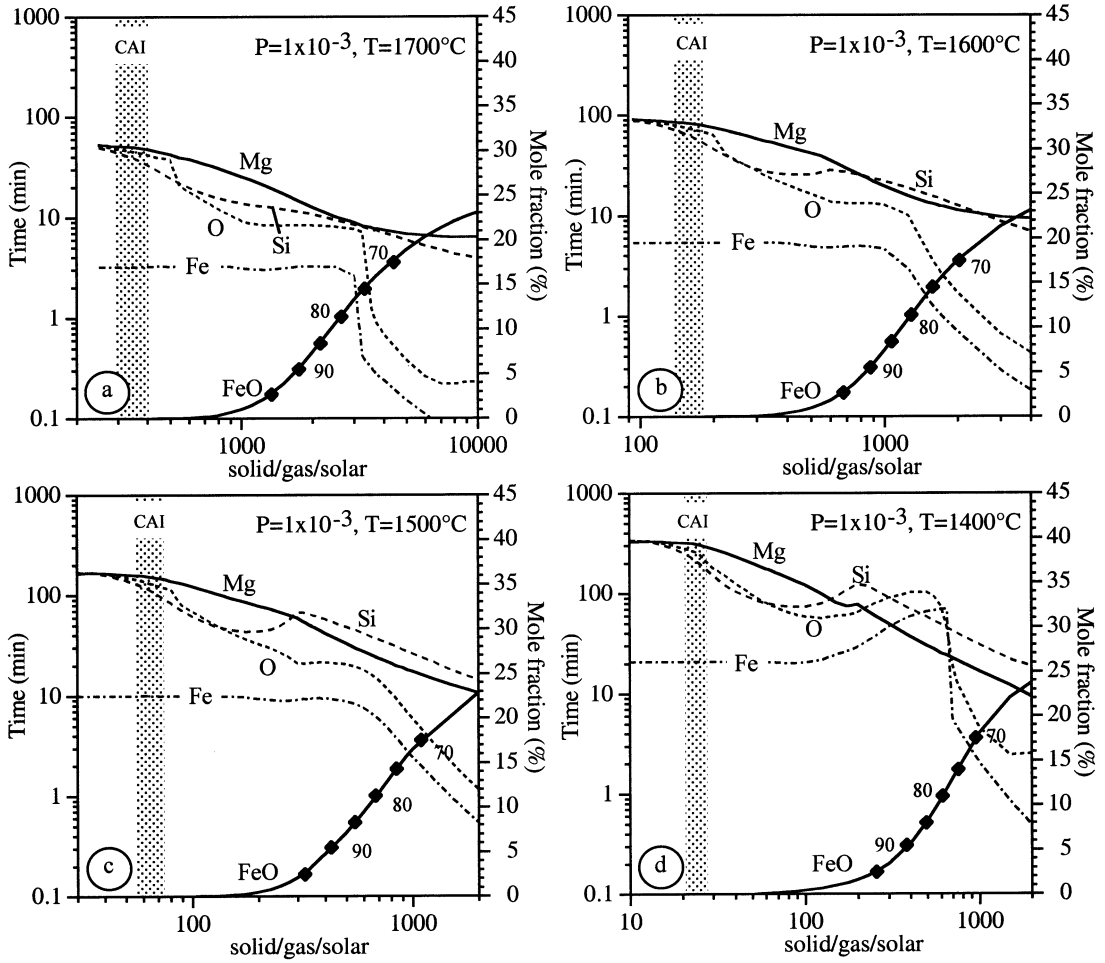

Fig. 10. The times (minutes) required in the EQR model to reach the maximum isotopic mass fractionations of O, Mg, Si and Fe in the silicate melts when $P_{tot} = 10^{-3}$ bars. To estimate times at lower for P_{tot}, divide both the times and solid/gas/solar ratios by $\sqrt{P_{tot}*1000}$. Also shown for reference is the region where CAI-like silicate compositions would form, and the FeO content (mole %) and the Mg# of the silicate melts.

At temperatures of 1600°C and below, prominent local maxima occur in the Si curves in Figures 9–12 at solid enrichments where the silicate compositions have Mg# of ~95. At Mg# of ≥98 there is a transition from the MELTS to the Berman (1983) CMAS melt solution models. At temperatures of ≤1600°C, the activities predicted by the two models at this transition are not very different. However, the α coefficients associated with the two solution models were determined at temperatures of 1700°C and above, and their extrapolated values diverge with decreasing temperature (Table A1). Recent experiments suggest that the α coefficients for the CMAS model are reasonably accurate down to temperatures of 1500°C (see Fig. EA1). There have been no experiments that can be used to test the MELTS α coefficients at temperatures below 1700°C.

3.3.1. Chondrules

As has already been discussed, significant isotopic fractionations develop rapidly under conditions where chondrule-like silicate compositions are produced (Figs. 9 and 10). This is particularly true for type Is, but would also be true for type IIs. The fact that chondrules exhibit little or no isotopic fractionation either in bulk or in their phenocrysts, but still preserve elemental fractionations (e.g., Fig. 6), means that they were able to equilibrate isotopically with the gas at high temperatures.

If we assume that chondrules cooled at 5 to 1000°C/h between 1600°C and 1400°C, this gives formation times of 12–2400 min. These times do not include chondrule heating times, so they are lower limits. Under almost all conditions, Fe reaches its maximum mass fractionations faster than O, Mg or Si (Figs. 9 and 10). The times for Fe to reach maximum mass fractionations vary with conditions, but are typically a few tens of minutes or less. Even at 1400°C and $P_{tot} = 10^{-4}$ bars, when evaporation rates are slowest under the range of conditions assumed here, 12 min would be sufficient to produce at least 1‰/amu Fe mass fractionation in most chondrules. This time is an upper limit for formation times if largely molten chondrules remained more or less closed to anything other than alkali loss. Preventing alkali

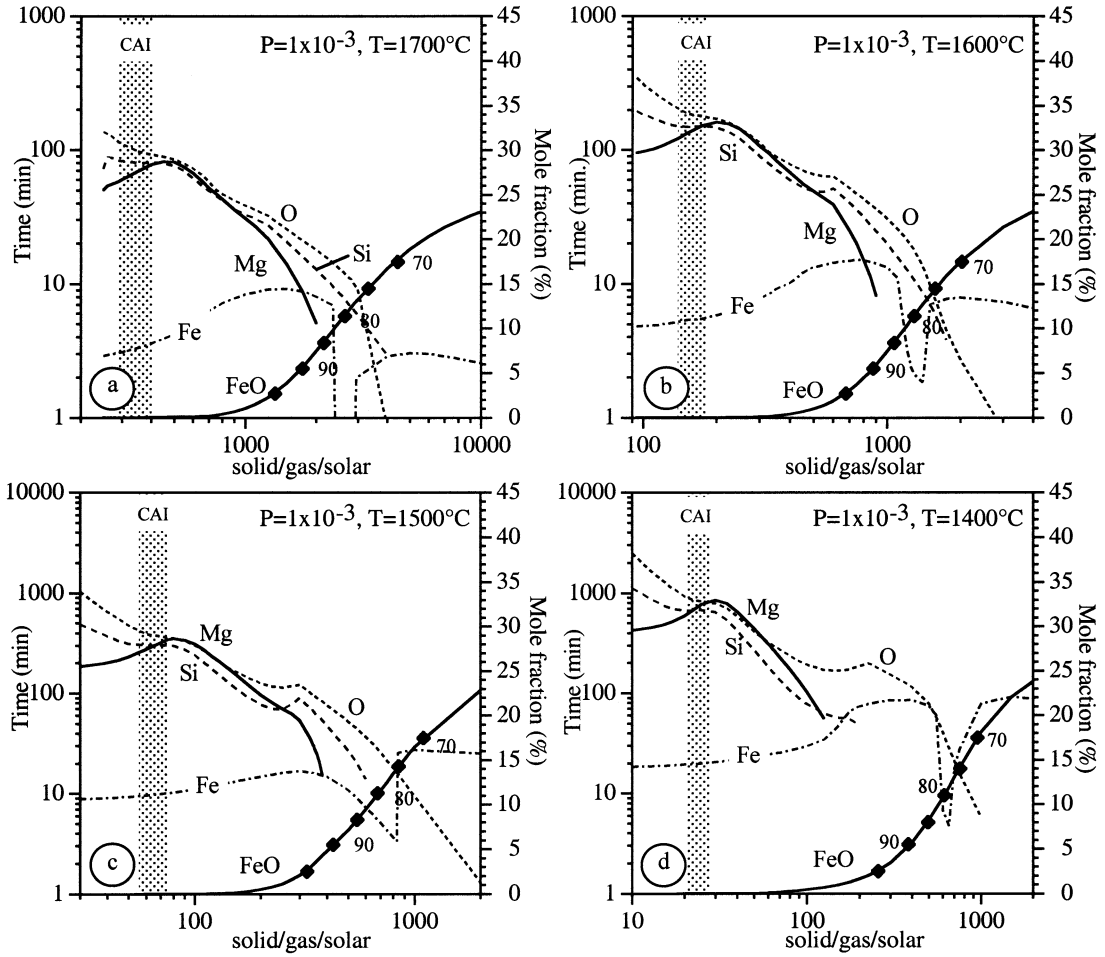

Fig. 11. The times (minutes) required in the PCR model for the isotopic mass fractionations in O, Mg, Si and Fe in silicate melts to fall below 0.25‰/amu when $P_{tot} = 10^{-3}$ bars. To estimate times at lower for P_{tot}, divide both the times and solid/gas/solar ratios by $\sqrt{P_{tot}*1000}$. At high solid/gas/solar ratios the mass fractionation may never have exceeded 0.25‰/amu. The slowest element provides an estimate of the equilibration time of the system under the assumed conditions. Also shown for reference is the region where CAI-like silicate compositions would form, and the FeO content (mole %) and the Mg# of the silicate melts. The sudden increase in equilibration times for Fe at dust to gas ratios where the Mg# ≈ 0.75 is due to significant negative mass fractionation associated with condensation of Fe from the gas. The Fe in the gas is mostly derived from evaporated metal.

loss requires even more rapid heating and cooling (Yu and Hewins, 1997; Alexander et al., 2000).

Heating and cooling in on the order of minutes for chondrules seem to be ruled out by experimental simulations of chondrule textures. Heating times of at least 10s of minutes would seem to be required, in which case there would have been significant evaporation and much larger isotopic mass fractionations would have developed in chondrules than are now observed. Therefore, formation times must have been long enough for chondrules to partially evaporate and then approach isotopic equilibrium with the gas.

Equilibration times depend on the element, the temperature and the total pressure. Equilibration of Fe is rapid, ~10–200 min depending on the conditions and model. The longer times occur at 1400°C when equilibration between metal and silicates via evaporation/condensation is slow. Thus, Fe would certainly equilibrate with the gas provided that the cooling rate was ≤60°C/h between 1600°C and 1400°C, but the cooling rates could probably be significantly faster. Erasing all mass fractionation in O, typically the slowest element to equilibrate, might need cooling rates as low as 5 to 20°C/h for the most magnesian chondrules.

3.3.2. *Calcium-Aluminum-Rich Inclusions*

For a Type B CAI starting composition, the mineralogy and textures of Type B CAIs are best reproduced by heating to temperatures of 1400 to 1550°C and subsequently cooling at rates of 0.5 to 50°C/h (Stolper, 1982; MacPherson et al., 1984; Stolper and Paque, 1986). Assuming that Type B CAIs cooled at 0.5 to 50°C/h between 1500°C and 1400°C, gives timescales of 120–12,000 min.

The model best reproduces the isotopic compositions of CAIs for temperatures between 1500°C and 1400°C, when the melts are able to partially reequilibrate with the gas. If CAIs formed in the way assumed here, formation timescales must be

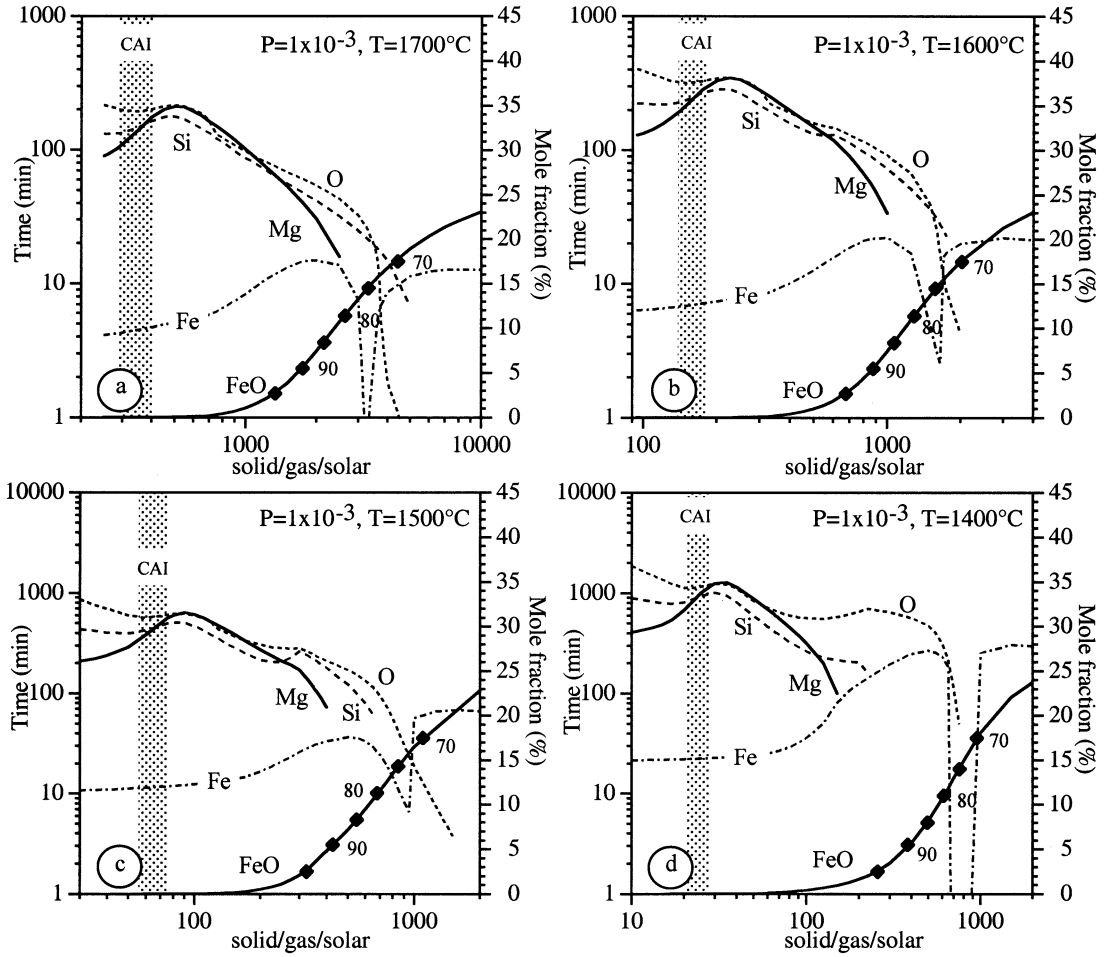

Fig. 12. The times (minutes) required in the EQR model for the isotopic mass fractionations in O, Mg, Si and Fe in silicate melts to fall below 0.25‰/amu when $P_{tot} = 10^{-3}$ bars. At high solid/gas/solar ratios the mass fractionation may never have exceeded 0.25‰/amu. To estimate times at lower for P_{tot}, divide both the times and solid/gas/solar ratios by $\sqrt{P_{tot}*1000}$. For more details see Figure 11.

between the time taken to reach the maximum isotopic fractionation (Figs. 9 and 10) and the equilibration time (Figs. 11 and 12). The CAI-like objects in these calculations are of the order of 0.2 mm in radius, at least an order of magnitude smaller than typical Type B CAIs in CV chondrites. If Type Bs evolved as discreet droplets (i.e., they are not compound), the times in Figures 9–12 will need to be increased by roughly an order of magnitude.

Under the conditions envisioned for CAI formation, times scale approximately inversely with $\sqrt{P_{tot}*1000}$. To produce Type B-sized objects ($r = 2$ mm) at 1500°C, the times needed to reach the maximum isotopic fractionation range from roughly 1000 to 5000 min at $P_{tot} = 10^{-3}$ (PCR model) and 10^{-4} (EQR model) bars, respectively. At 1400°C, these times increase to roughly 3000 and 10,000 min, respectively. Equilibration times at 1500°C are ~3000–20,000 min, and at 1400°C are ~10,000–40,000 min for the same range of total pressures. These times are consistent with the times estimated from the cooling rates, particularly for cooling rates and total pressures at the lower ends of the ranges considered.

Total pressures close to 10^{-4} bars would be more consistent with astrophysical models. Evaporation rates are relatively slow at such pressures, so that diffusion in the melt has a minor influence on isotopic fractionation even for centimeter-sized objects (Richter et al., 2002). Even at 10^{-3} bars, the influence of diffusion is modest. Total pressures could not be much lower than 10^{-4} bars, otherwise the times needed to reach the maximum isotopic compositions become too long.

4. O MASS INDEPENDENT FRACTIONATIONS

The pervasiveness of O mass independent fractionations (MIFs) in early Solar System materials at scales from micron-sized grains to planets is an indication of the importance of this mysterious phenomenon. The main O-bearing species in the nebula were silicates, H_2O and CO. It is generally believed that the O isotopic compositions of chondrules and CAIs were established via gas-solid/melt exchange between these reservoirs (Thiemens, 1988; Clayton, 1993). The isotopic compositions of the three reservoirs before and during chondrule/CAI formation remain unresolved, as do when and how they were established.

Three possible ways of producing MIF in one or more of the main O reservoirs have been proposed. The MIF could have been inherited from the presolar molecular cloud. Clayton (1988) suggested that on average dust in the interstellar medium (ISM) will be older than the gas. As a result of galactic chemical evolution, O in the Galaxy has become on average less ^{16}O-rich with time. If on average the dust were older, it would have been more ^{16}O-rich than the gas and the bulk system. On the other hand, due to the self-shielding effect, preferential UV photodissociation of $C^{17,18}O$ in the presolar molecular cloud may have produced ^{16}O-poor water ice mantles on all silicate grains (Yurimoto and Kuramoto, 2002). Enrichment of the ice-silicate grains relative to the gas in the nebula, followed by heating of the grains would result in exchange between a ^{16}O-poor gas and ^{16}O-rich silicates.

Another suggestion is that self-shielding during UV irradiation of CO led to the preferential dissociation of $C^{17,18}O$ in a limited region of the solar nebula near the Sun (Clayton, 2002a,b). The O liberated by this process would have reacted to form H_2O, creating a ^{16}O-poor O and H_2O reservoir, and a ^{16}O-rich CO reservoir. The O and H_2O would preferentially exchange with dust. To explain the range of O isotopic compositions in Solar System objects in this way requires: (i) that the bulk Solar System has a composition that is similar to the most ^{16}O-rich compositions in CAIs, and (ii) that, with the exception of CAIs, almost all inner Solar System material underwent this processing. Why CAIs or their precursors escaped this processing is not explained. After processing in this region, the material was redistributed throughout the inner Solar System, perhaps by an X-wind (Shu et al., 1996, 1997, 2001).

The third explanation proposes that the MIF was the product of non-RRKM intramolecular kinetic isotope (mass independent) effects during gas phase reactions in the nebula. Whether this MIF took place before or during chondrule/CAI formation is not known. The best known means for producing MIF is the formation and dissociation of ozone under various conditions, but a number of other reactions have been identified that produce this effect (Thiemens, 1999; Weston, 1999). It is possible that many more exist. Of the known MIF producing reactions, at least one,

$$CO + OH = CO_2 + H, \qquad (R3)$$

played an important role in the nebula (see below).

As with the previous explanation, the non-RRKM kinetic isotope explanation produces two gaseous reservoirs with opposite MIFs. To transfer the MIF of one of these reservoirs to the chondrule/CAI, either requires that one of them exchanged more rapidly with the chondrules/CAIs than any other O-bearing species, or that one of the reservoirs was fractionated along with the solids from the remaining gas.

Here, the results described in previous sections along with the kinetics of gas-gas exchange are used to test three basic models that incorporate the essential features of the three explanations for the MIF. These models are: (A) before chondrule/CAI formation, MIFs of opposite sign were established in CO and H_2O, (B) the initial silicate composition was $\delta^{17,18}O = -50‰$ and it exchanged with a ^{16}O depleted gas, and (C) MIFs of opposite sign were established in two or more gaseous components during chondrule/CAI formation.

4.1. Model A: Gas-Gas Equilibration Times

The self-shielding model as proposed by Clayton (2002a,b) relies on H_2O exchanging with silicates more rapidly than CO, and that H_2O-silicate exchange is faster than H_2O-CO reequilibration. An alternative, also requiring faster exchange by H_2O than by CO, would be that the H_2O were ^{16}O-rich and the CO ^{16}O-poor. In this case, the initial silicate and bulk solar compositions could lie on the terrestrial fractionation line, and the chondrules/CAIs become ^{16}O-rich by exchange with the H_2O. The attraction of having a bulk composition near the terrestrial mass fractionation line is that most large Solar System bodies have compositions that lie near the terrestrial mass fractionation line. This includes CI and enstatite chondrites. There was probably little or no water in the region where the enstatite chondrites formed. The simplest explanation for the enstatite chondrite isotopic compositions is that they closely resemble the composition of the bulk silicates plus some CO, although, if there was MIF in the H_2O and CO, the composition of the H_2O-rich CIs requires H_2O-CO exchange before CI formation.

If there was no fractionation of H_2O from CO, the success or failure of both explanations rests on the CO-H_2O isotopic equilibration times during chondrule/CAI formation. If CO-H_2O equilibration times are shorter than the gas-melt equilibration times, model A is ruled out. As will be discussed in more detail below, an essential feature for model C is also that the reactions producing the MIF do not approach equilibrium.

The numerical simulations show that, at high temperatures and under relatively oxidizing conditions, H_2O would have interacted with a melt more rapidly than CO via evaporation/condensation reactions [e.g., $SiO_{(g)} + H_2O_{(g)} = SiO_{2(l)} + H_2$]. Nevertheless, CO-melt exchange does occur and becomes increasingly important as the H_2O/CO ratio decreases. At high temperatures when silicate-gas exchange will be fastest, atomic O reacts rapidly to form OH and H_2O, so it is unlikely to exchange directly with the silicates to any significant extent.

Isotopic equilibration rates in the gas were determined by giving the initial CO and H_2O opposite mass independent anomalies. The sizes of the anomalies were calculated so that at equilibrium the bulk $\delta^{18}O = 0‰$. No evaporation-condensation or gas-melt exchange is allowed during these calculations, but the H_2O, C, and excess O from the CI dust is put into the gas at the start of the integration. Hence the results depend on the solid/gas/solar ratio. In the model, during equilibration the anomalies in CO and H_2O decay exponentially at very similar rates. From fits to the model results, to a good approximation the decay constant for the equilibration is given by

$$\lambda\left(\mathrm{min}^{-1}\right) \approx \sqrt{P_{tot}}\left(-2.199 \times 10^4 \times D_g^2 + 1.892 \times 10^8 \times D_g + 8.131 \times 10^8\right) \times e^{-35119/T}. \qquad (5)$$

One over λ, the characteristic time, is a convenient measure of the equilibration time (Fig. 13).

The value of the decay constant is highly correlated with the partial pressure of OH, suggesting that one of the reactions

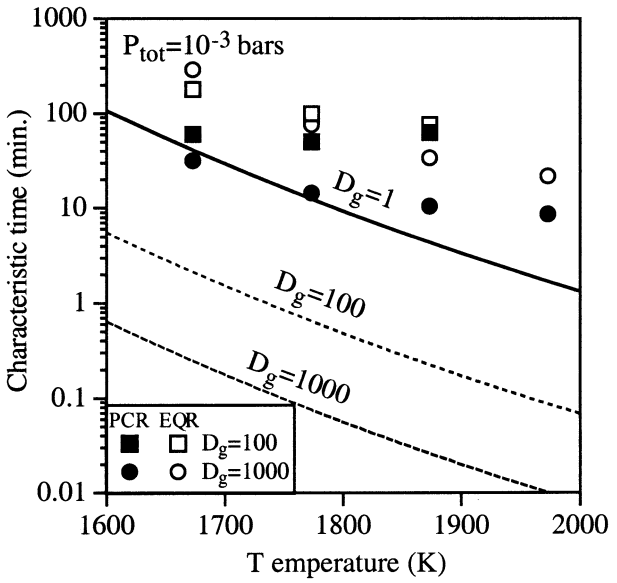

Fig. 13. The characteristic times (minutes) for CO-H_2O (curves) and gas-melt (points) O isotope equilibration as a function of temperature, and solid/gas/solar ratio for $P_{tot} = 10^{-3}$ bars. The curves were calculated with Eqn. 5. The gas-melt characteristic times were calculated in the simulations described in the text. The initial particle radius for the melt was 0.468 mm. Gas-melt equilibration times will scale with the initial radius of the particles.

involving OH (Table A2) determines the equilibration rates. The most likely of these, since it also involves CO, is the reaction R3.

An alternative means of estimating equilibration timescales, assuming R3 is the rate determining step, can be obtained from the rate at which CO would be consumed by the reaction (J. Lyons, private communication), i.e.,

$$\frac{d[CO]}{dt} = -k_{CO-OH}[OH][CO]. \quad (6)$$

In this case, $k_{CO\text{-}OH}[OH]$ can be thought of as the decay constant. Combining a fit to the equilibrium partial pressures of OH calculated in the simulations with the rate coefficient for this reaction (Table A2) gives

$$k_{CO-OH}[OH](min^{-1}) = \sqrt{P_{tot}}(-1328 \times D_g^2 + 4.804 \times 10^6 \times D_g + 1.012 \times 10^7) \times e^{-34381/T} T^{0.5}. \quad (7)$$

The characteristic times for equilibration predicted by Eqn. 7 are in close agreement with the numerical results (Eqn. 5). They are also faster than for gas-melt exchange of chondrule-sized or Type-B-CAI-sized objects (Figs. 11 and 12). Thus, gas-gas equilibration would erase any preexisting MIF between gas phases before it could be transferred to chondrules or CAIs. Gas-melt exchange would only be comparable to gas-gas equilibration if the melt were present as particles that were at least 1–2 orders of magnitude smaller than assumed here. Semiquantitative arguments led Navon and Wasserburg (1985) and Lyons and Young (2003) to similar conclusions.

One way to overcome the requirement that gas-silicate exchange is faster than gas-gas exchange would be to fractionate H_2O and silicates from the CO before chondrule/CAI formation. The Clayton (2002a,b) self-shielding model does not consider the possibility of fractionating H_2O from CO. Presumably this is because it would require the formation of ice, and the self-shielding occurs near the Sun where ambient temperatures would be above the ice condensation temperature. However, the presolar molecular cloud (Yurimoto and Kuramoto, 2002) and cooler high altitude regions of the nebula where the UV light can penetrate are places where self-shielding could occur. The H_2O that is produced in these regions would freeze out. Fractionation of the ice and dust from the CO would create a situation like that of Model B. Young and Lyons (2003) have recently begun to quantitatively explore the possibility of self-shielding operating at high altitudes in the outer part of the early Solar System.

4.2. Model B: MIF between Gas and Dust

Clayton and Mayeda (1984) first proposed that primordial dust had a composition near the most ^{16}O-rich compositions found in CAIs and that the bulk nebula gas was ^{16}O-poor. Galactic chemical evolution and self-shielding accompanied by ice fractionation, amongst other suggestions, provided explanations for how such gas and dust compositions might be produced.

Chondrules and non-FUN CAIs with modest isotopic mass fractionations probably approached equilibrium with the ambient gas. In this case, the ultimate composition of chondrules or CAIs depends on the solid/gas/solar ratio where they formed. Figure 14 shows the bulk O isotopic compositions for various solid/gas/solar ratios assuming a bulk solar O composition of $\delta^{17,18}O = 0‰$, a solid composition of $\delta^{17,18}O = -50‰$ and a gas composition of $\delta^{17,18}O = 24‰$. For $P_{tot} = 10^{-3}$ bars and T = 1400°C, the lowest solid/gas/solar ratio at which non-FUN CAI-like elemental compositions would form is $D_g \approx 20$. At lower total pressures, the solid/gas/solar ratio needed to produce the same CAI-like elemental composition increases. The O isotopic composition at $D_g = 20$ in Figure 14 is the upper limit for the bulk $\delta^{17,18}O$ values of CAIs for these end member compositions. Even after correcting for mass fractionation that may have pulled the CAIs away from the slope 1 line, most of them have much higher bulk $\delta^{17,18}O$ values than this. The CAI compositions could be explained if the gas compositions were much more $^{17,18}O$-rich than assumed above, but there is little evidence for a reservoir of this composition in any other Solar System materials.

Previously, it was shown that chondrules must have formed at much higher solid/gas/solar ratios than CAIs. If we assume the above initial solid and gas compositions for chondrules, they would exhibit more extreme ^{16}O enrichments than CAIs, which they do not. Two ways to reconcile the chondrule compositions with a Clayton-Mayeda-type model are either for chondrules to have formed from precursors that had already exchanged with a gas at near or subsolar solid/gas ratios, or chondrules exchanged with a much more ^{16}O–poor gas than CAIs. At present, there is no direct evidence that either occurred.

Another possibility is suggested by the fact that if the "volatile" O in the CI composition (see section 2.5) has a composition of $\delta^{17,18}O \approx 0‰$ and the refractory O $\delta^{17,18}O \approx -50‰$,

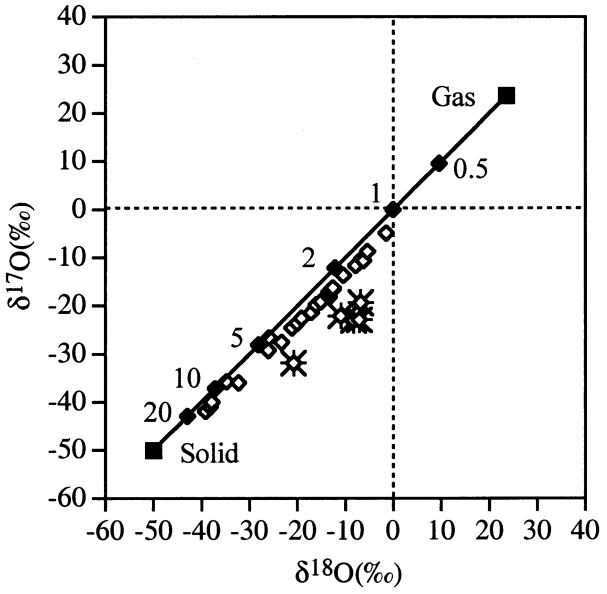

Fig. 14. The bulk O isotopic compositions of CAIs (open symbols, FUN inclusions are starred). The CAI data are from Clayton et al. (1987, 1988), but with all inclusions with negative Si mass fractionation excluded (Grossman et al., 2000). Also shown are the mean O isotopic compositions after gas-melt equilibration for various (numbered) solid/gas/solar ratios, assuming a bulk solar O composition of $\delta^{17,18}O = 0‰$, an initial solid composition of $\delta^{17,18}O = -50‰$ and an initial gas composition of $\delta^{17,18}O = 24‰$. For $P_{tot} = 10^{-3}$ bars and T = 1400°C, the lowest solid/gas/solar ratio at which non-FUN CAI-like compositions would form is $D_g \approx 20$. At lower total pressures and/or higher temperatures, the solid/gas/solar ratios needed to produce non-FUN CAI-like compositions increase.

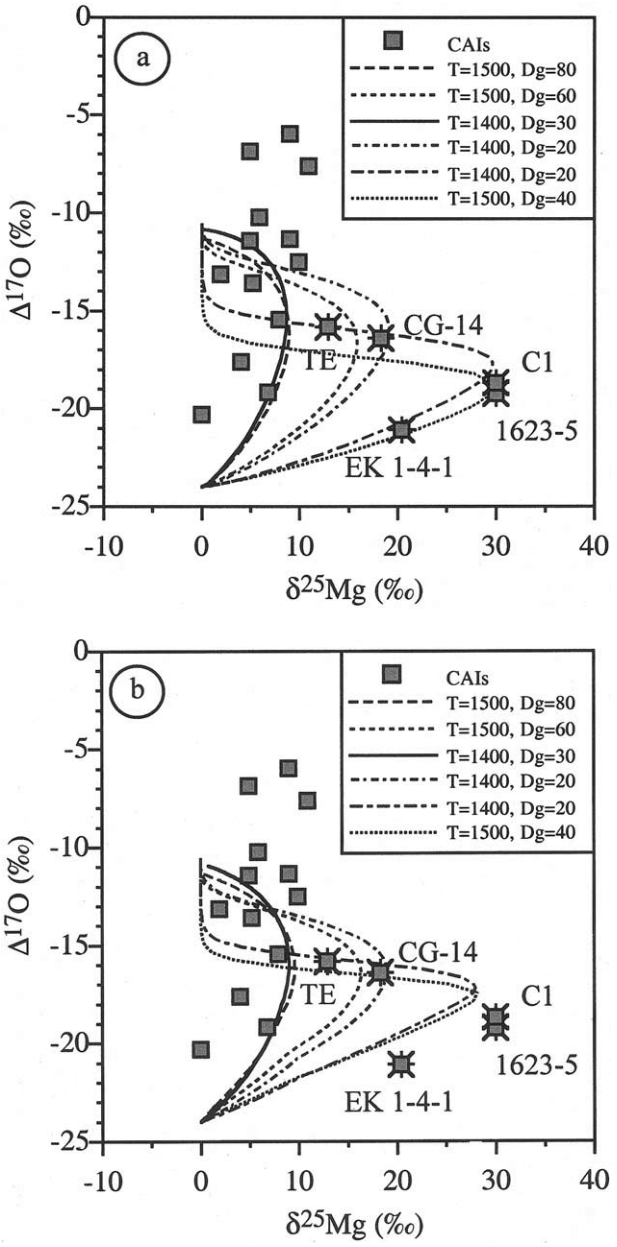

Fig. 15. Comparison of bulk CAI isotopic compositions (symbols, FUN inclusions are starred) with (a) PCR and (b) EQR model evolution paths under various conditions. The precursor silicates are assumed to have a composition of $\delta^{17,18}O = -50‰$, and the gas and "volatile" O a composition of $\delta^{17,18}O = 0‰$. The "volatile" O is the O that is present in CI chondrites as water/OH, sulfates, carbonates and Fe-oxides.

the range of bulk CAI compositions is reproduced by the PCR model quite well (Fig. 15a), but less so by the EQR model (Fig. 15b). This "volatile" O could be ice that accompanied the cluster IDP-like dust. There is no reason why the "volatile" O should always occur in CI abundances or that its composition was exactly $\delta^{17,18}O = 0‰$, which may account for some of the differences between the model and the bulk CAIs. Because chondrule O isotopic compositions are closer to the terrestrial fractionation line, this explanation would require that chondrule precursors had higher ice/silicate ratios than CAI precursors.

It remains to be seen whether this explanation can reproduce the internal O isotope systematics of CAIs, if indeed they are primary. Spinel, fassaite etc. typically exhibit the most ^{16}O-rich compositions and little O mass fractionation (Clayton, 1993). If the precursor material were solar, by the time enough mass loss has occurred to enable these minerals to crystallize, the O isotopic composition may be highly mass fractionated or have experienced substantial isotopic exchange with the ^{16}O-depleted gas.

4.3. Model C: MIF Generated during Chondrule/CAI Formation

Numerical simulations have shown that if H_2O were ^{16}O-rich, it would transfer this ^{16}O enriched composition to the silicates. If the CO in the system were ^{16}O-poor, then the bulk solar composition could lie near the terrestrial fractionation line. However, as was shown above, gas phase reactions quickly erase any preexisting MIF between H_2O and CO. One way of overcoming this is if the MIF between H_2O and CO is generated during chondrule/CAI formation, possibly as a result of non-RRKM kinetic isotope effects or self-shielding. Assuming that the MIF is produced during chondrule formation, simulations suggest that for reasonable peak temperatures and cooling rates ^{16}O enrichments can be produced in a melt at high temperatures and then evolve back towards more normal isotopic compositions as the system cools. If this is to occur, then:

(1) large ^{16}O enrichments must be continuously generated in H_2O and ^{16}O depletions generated in CO, and (2) at lower temperatures either the mechanism for generating the MIFs switches off and/or CO exchanges faster than H_2O at lower temperatures when direct gas-melt exchange becomes more important. However, little is known of the absolute and relative rates of direct CO- or H_2O-melt O isotopic exchange, and the size of the ^{16}O enrichments in the melts depends on the size of the MIFs that are assumed to develop in the CO and H_2O.

In the case of self-shielding, the dissociation rates would have to significantly exceed the gas-gas equilibration rates. Whether this is possible at the high temperatures of CAI formation remains to be seen. The MIF effects of self-shielding for O_2 are quenched above 500 K (Navon and Wasserburg, 1985). In the absence of estimates of UV fluxes and dissociation rates for the various molecular species in the gas, self-shielding cannot be tested here.

Of the reactions known to produce MIF in O, reaction R3 is likely to be the most relevant to the nebula. However, Thiemens (1999) suggests that any reaction involving a symmetric O-M-O structure, such as ozone and CO_2, either as a product/reactant or as an intermediate state, will produce MIF. Other candidate reactions for producing MIF, because they involve such symmetric molecules or they resemble reaction R3, include: $SiO + OH = SiO_2 + H$, $O_2 + Mg = MgO + O$, $O + OH = O_2 + H$, $O_2 + Al = AlO + O$. The rates for all of these reactions are available and have been included in the gas phase reaction network (see Table EA2). Abundances of CaO, FeO and AlO_2 in the nebula are likely to be very low, and reactions involving them are not considered.

Two important features of the non-RRKM kinetic isotope effect need to be borne in mind—MIF is produced in both products and reactants, and the reactions listed above are all reversible. Take reaction R3,

$$C^iO + {}^jOH = C^iO^jO + H,$$

as an example. The assumption adopted here is that the reaction is faster when $i = j = 16$ than for any other combination of masses. When going from left to right, the reaction will make CO_2 that is ^{16}O-rich, as well as CO and OH that are ^{16}O-poor. The enrichments and depletions that are generated will depend on the relative abundances of the three O-bearing gas species and how far the reaction has proceeded. If the reaction is fully reversible, as it is in this case, the reaction from right to left must also be faster when $i = j = 16$ than for any other combination of masses. As a result, at equilibrium there will be no net MIF between products and reactants.

For the non-RRKM kinetic isotope effect operating during chondrule/CAI formation to be the explanation, several things must happen. The reaction(s) producing the MIF must not approach equilibrium. Assuming it is the product that has the desired MIF, the product-silicate exchange must be faster than any other O-bearing gas-silicate exchange. Silicate-product exchange must also be faster than exchange between the product and other gas species. Finally, the size of the MIF in the product must be large enough to overcome the diluting effects of the silicates' initial O isotopic composition and silicate exchange with other gas species.

Numerical simulations suggest that under the chondrule/CAI formation conditions assumed in this work, none of the reactions considered here meet all the criteria listed above. All gas phase reactions approach equilibrium fairly rapidly compared to gas-melt exchange. Other than for reaction R3, all the products and reactants are relatively minor constituents of the nebula. Even if they carried MIF O and exchange with the silicates, their contribution would be overwhelmed by the exchange with H_2O and, to a lesser extent, CO via evaporation-condensation reactions.

For the non-RRKM kinetic isotope effect to work, it must induce MIF in H_2O and/or CO. Reaction R3 is the best candidate for doing this because it directly involves CO and any MIF that is induced in OH is transferred to H_2O quite quickly. However, its rapidity also means that it approaches equilibrium very quickly. As a result, the MIF that does develop at the beginning of a simulation is small and transient. Also, the abundance of CO_2 compared to CO and H_2O (via OH) is very small. To induce significant MIF in CO and H_2O, mass balance would require huge anomalies in the CO_2, which seems unlikely. Similar mass balance arguments plague the other reactions because either the reactant or the product have relatively low abundances.

The only way for the non-RRKM kinetic isotope effect to produce the MIF during chondrule/CAI formation is if there was a process that prevented the gas from approaching equilibrium. One way of doing this is to have a source of radiation that can dissociate or ionize components in the gas. Mass independent fractionation is also known to occur in ion-molecule reactions (Weston, 1999). The radiation fluxes associated with cosmic rays and radioactive decay are probably too small to influence chondrule/CAI formation. The initial pulse of electrons and UV radiation during a lightening discharge would be too short to prevent gas equilibration over the minutes to hours needed to form chondrules and CAIs (Desch and Cuzzi, 2000). At chondrule/CAI formation temperatures, partial ionization of the alkalis would produce some ions and free electrons. Recombination will largely take place on grain surfaces (S. Desch, private communication). The lower initial solid densities and higher degrees of evaporation in CAI formation regions might explain why CAIs exhibit more MIF. Finally, qualitatively the X-wind model does predict intense radiation fluxes in the CAI formation region and lower fluxes in the chondrule forming region (Shu et al., 1996, 1997, 2001). However, CAIs would form in an almost gas-free environment, and to date the model makes few quantitative predictions about the times and conditions during CAI and chondrule formation, so it cannot be tested here.

In the absence of an external radiation source during chondrule/CAI formation, perhaps the most likely setting for the non-RRKM kinetic isotope model is not during chondrule/CAI formation, but at low temperatures either in the precursor molecular cloud or the solar nebula. Under these conditions, equilibration in the gas would be slow and if H_2O is produced with MIF it could freeze out as ice and be fractionated with the dust from the gas, as in model B.

5. SUMMARY AND CONCLUSIONS

Recently, it has been suggested that the isotopic compositions of chondrules and CAIs required total pressures that are

unlikely to have existed at 2–3 AU in the solar nebula. However, these studies did not take into account the effects of melt-gas exchange. To determine whether melt-gas exchange could allow chondrules and/or CAIs to form under conditions that astrophysical models predict for 2–3 AU, a kinetic evaporation-condensation model has been developed and calibrated against a number of evaporation experiments. Assuming a CI-like precursor bulk composition, a large number of simulations have been conducted over a range of conditions that are consistent with a canonical solar nebula at 2–3 AU (P_{tot} = 10^{-4}-10^{-3} bars, T = 1400 to 1700°C, and solid/gas/solar = 10–60,000).

For this initial study, it was necessary to make a number of simplifying assumptions because some processes are not well understood and to keep the number of free parameters to a reasonable number. Perhaps the two most important of these are: (1) ignoring crystallization/dissolution, and (2) assuming isothermal, isobaric conditions. Crystallization/dissolution was ignored because the kinetics of this process is very poorly understood, and on the assumption that most evaporation/condensation occurred at near liquidus temperatures. Introducing more complex temperature and pressure regimes opens up a potentially huge phase space that would be better explored in the context of specific formation models.

The relative importance of the various simplifying assumptions made here will have to be assessed in future studies. Nevertheless, the first order results presented here show that most chondrules and molten CAIs could have formed in a canonical solar nebula, albeit with significant local solid/gas enrichments, at 2–3 AU from CI-like precursors, although some chondrules and molten CAIs may have formed from fractionated precursors. The "equilibrium" compositions, isotopic mass fractionations and equilibration times are compared to chondrule/CAI compositions and inferred formation times to better constrain their formation conditions.

The lack of large isotopic mass fractionations in any element in chondrules suggests that they approached equilibrium with their environment when they formed. For all the conditions where chondrule-like "equilibrium" silicate melt compositions are produced, the calculated equilibration times are consistent with chondrule formation times inferred from their textures. Assuming CI-like precursor compositions, "equilibrium" silicate melts with elemental compositions like those of type A chondrules could have formed over a range of conditions (T, P_{tot}, solid/gas/solar). At constant temperature, melts of similar composition can form over a restricted range of total pressures and solid/gas/solar ratios ($D_g\sqrt{\mathbf{P}_{tot}} \approx$ constant). Thus, chondrule compositions can be used to constrain the pressures and solid/gas/solar ratios they formed at if the temperature is known.

The compositions of type B chondrules, Al-rich chondrules and Type C CAIs cannot be explained as "equilibrium" melts under the conditions assumed here. They may have formed either: (1) in regions where precursors were on average more silica-rich than CI, or (2) from individual, fractionated precursors whose bulk compositions were not homogenized, but whose components (minerals and glass) approached equilibrium with a system that as a whole was unfractionated.

The abundances and compositions of metal in chondrules are less successfully reproduced than the silicate compositions, perhaps because the precursors of type I chondrules were more reduced than CI, and there was metal-silicate fractionation before formation of type II chondrules.

CAI formation conditions are more tightly constrained than for chondrules. This is because at a given temperature and pressure, Mg abundances fall rapidly with decreasing solid/gas/solar ratio in the region where CAI-like elemental compositions form. The isotopic mass fractionations in non-FUN CAIs can be reproduced if they formed in these regions at ~1400 to 1500°C ($D_g\sqrt{P_{tot}\times 1000}$ = 20 − 30 at 1400°C and 60–80 at 1500°C), but did not quite reach equilibrium with the gas. Formation times at total pressures of 10^{-4}-10^{-3} bars are consistent with estimates of Type B CAI cooling times, but pressures much below this range would require formation times that are too long.

The isotopic mass fractionations in FUN CAIs can be explained if they formed at or below the lower edge of the range of solid/gas/solar ratios for making CAI-like equilibrium compositions. The FUN CAI formation temperatures are less well constrained than for non-FUN CAIs. Most are consistent with formation at 1400 to 1500°C, but higher temperatures cannot be ruled out.

Various explanations for the origin of the O mass independent fractionations (MIF) in chondrules and CAIs have also been examined. These can be divided into two general approaches: creation of the MIF before chondrule/CAI formation, and creation of the MIF during chondrule/CAI formation.

Creation of MIF between H_2O and CO in a solar composition gas before chondrule/CAI formation followed by preferential H_2O-melt exchange can be ruled out. This is because H_2O-CO equilibration is faster than H_2O-melt exchange. The formation of CAI MIF compositions by exchange between ^{16}O-rich CI-like solids and ^{16}O-poor nebula gas is also unlikely. At the solid/gas/solar ratios needed to reproduce the isotopic mass fractionations in CAIs, the solid is the dominant O reservoir. Consequently, to reproduce the CAI O isotope systematics the gas compositions would have to have been much more ^{16}O-poor than any known reservoir. Chondrules would have formed at even higher solid/gas/solar ratios, requiring either even more extreme gas compositions, or gas-silicate exchange at or near solar solid/gas ratios before formation. If the MIF was established before chondrule/CAI formation, the most promising explanation is that H_2O (presumably as ice) and anhydrous silicates with MIFs of opposite sign are fractionated together from the remaining gas. Then on heating the ice goes into the gas and exchanges with the melt.

During chondrule/CAI formation, H_2O-melt exchange via evaporation-condensation reactions dominates the gas-melt O exchange. Consequently, if the MIF was generated during chondrule/CAI formation, it must be generated in the H_2O. To create a large MIF in the H_2O, mass balance requires creation of MIF of opposite sign in CO. Self-shielding from UV radiation is capable of doing this at low temperatures, but the effect may be quenched at high temperatures. Non-RRKM kinetic isotope effects are also capable of inducing MIF between H_2O and CO, but only if the gas phase reactions are prevented from approaching equilibrium. Preventing equilibration in the gas phase at chondrule/CAI formation temperatures and pressures

probably requires a continuous source of radiation that can dissociate or ionize the gas.

Acknowledgments—The Author would like to thank F. Richter for generously sharing unpublished results for numerous evaporation experiments, and G. MacPherson for sharing his CAI and Al-rich chondrule database. The author is also grateful to M. Thiemens, J. Wasson and H. Connolly for helpful discussions during the course of this work. H. Connolly, H. Yurimoto, S. Russell and an anonymous reviewer helped greatly improve this manuscript. The work was partially funded by NASA Origins of Solar Systems grant NAG5-13040.

Associate editor: S. S. Russell

REFERENCES

Alexander C. M. O'D. (1996) Recycling and volatile loss in chondrule formation. In *Chondrules and the Protoplanetary Disk* (eds. R. H. Hewins, R. H. Jones, and E. R. D. Scott), pp. 233–242. Cambridge University Press.

Alexander C. M. O'D. and Grossman J. N. (2000) The K isotopes in Semarkona chondrules. *Lunar Planet. Sci.* **31,** 1850.

Alexander C. M. O'D. (2001) Exploration of quantitative kinetic models for the evaporation of silicate melts in vacuum and hydrogen. *Meteor. Planet. Sci.* **36,** 255–284.

Alexander C. M. O'D. (2002a) Application of MELTS to kinetic evaporation models of FeO-bearing silicate melts. *Meteor. Planet. Sci.* **37,** 245–256.

Alexander C. M. O'D. (2002b) Exploration of a kinetic model for chondrule formation. *Lunar Planet. Sci.* **33,** 1864.

Alexander C. M. O'D., Grossman J. N., Wang J., Zanda B., Bourot-Denise M., and Hewins R. H. (2000) The lack of potassium isotopic fractionation in Bishunpur chondrules. *Meteor. Planet. Sci.* **35,** 859–868.

Alexander C. M. O'D., Boss A. P., and Carlson R. W. (2001) The early evolution of the inner solar system: A meteoritic perspective. *Science* **293,** 64–68.

Alexander C. M. O'D. and Wang J. (2001) Iron isotopes in chondrules: Implications for the role of evaporation during chondrule formation. *Meteor. Planet. Sci.* **36,** 419–428.

Allende Prieto C. A., Lambert D. L., and Asplund M. (2001) The forbidden abundance of oxygen in the Sun. *Astrophys. J.* **556,** L63–L66.

Allende Prieto C. A., Lambert D. L., and Asplund M. (2002) A reappraisal of the solar photospheric C/O ratio. *Astrophys. J.* **573,** L137–L140.

Anders E. and Grevesse N. (1989) Abundances of the elements: Meteoritic and solar. *Geochim. Cosmochim. Acta* **53,** 197–214.

Beckett J. R. (1986) The origin of calcium-, aluminum-rich inclusions from carbonaceous chondrites: An experimental study. Ph.D. thesis. University of Chicago.

Beckwith S., Sargent A. I., Chini R. S., and Güsten R. (1990) A survey for circumstellar disks around young stellar objects. *Astron. J.* **99,** 924–945.

Berman R. G. (1983) A thermodynamic model for multicomponent melts, with application to the system CaO-MgO-Al_2O_3-SiO_2. Ph.D. thesis. University of British Columbia.

Bischoff A. and Keil K. (1984) Al-rich objects in ordinary chondrites: Related origin of carbonaceous and ordinary chondrites and their consitituents. *Geochim. Cosmochim. Acta* **48,** 693–709.

Blander M., Unger L., Pelton A., and Ericksson G. (2001) Nucleation constraints lead to molten chondrule precursors in the early Solar System. *J. Phys. Chem. B* **105,** 11823–11827.

Boss A. P. (1996) Evolution of the Solar Nebula. III. Protoplanetary disks undergoing mass accretion. *Astrophys. J.* **469,** 906–920.

Boss A. P. (2000) Possible rapid gas giant planet formation in the solar nebula and other protoplanetary systems. *Astrophys. J.* **536,** L101–L104.

Bradley J. P., Keller L. P., Snow T. P., Hanner M. S., Flynn G. J., Gezo J. C., Clemett S. J., Brownlee D. E., and Bowey J. E. (1999) An infrared spectral match between GEMS and interstellar grains. *Science* **285,** 1716–1718.

Chase M. W. Jr. (1998) NIST-JANAF thermochemical tables fourth edition. In *J. Phys. Chem. Ref. Data*, Vol. Monograph 9, pp. 1963. AIP.

Choi B.-G., Huss G. R., Wasserburg G. J., and Gallino R. (1998) Presolar corundum and spinel in ordinary chondrites: Origins from AGB stars and a supernova. *Science* **282,** 1284–1289.

Chuang Y.-Y., Hsieh K.-C., and Chang Y. A. (1985) Thermodynamics and phase relationships of transition metal-sulfur systems: Part V. A reevaluation of the Fe-S system using an associated solution model for the liquid phase. *Metall. Trans. B* **16B,** 277–285.

Clayton D. D. (1988) Isotopic anomalies: Chemical memory of galactic evolution. *Astrophys. J.* **334,** 191–195.

Clayton R. N. (1993) Oxygen isotopes in meteorites. *Ann. Rev. Earth Planet. Sci.* **21,** 115–149.

Clayton R. N. (2002a) Photochemical self-shielding in the Solar Nebula. *Lunar Planet. Sci.* **33,** 1326.

Clayton R. N. (2002b) Solar System: Self-shielding in the solar nebula. *Nature* **415,** 860–861.

Clayton R. N., Grossman L., and Mayeda T. K. (1973) A component of primitive nuclear composition in carbonaceous meteorites. *Science* **182,** 485–488.

Clayton R. N. and Mayeda T. (1984) The oxygen isotope record in Murchison and other carbonaceous chondrites. *Earth Planet. Sci. Lett.* **67,** 151–161.

Clayton R. N., Mayeda T. K., Rubin A. E., and Wasson J. T. (1987) Oxygen and silicon isotopes in inclusions and chondrules from Vigarano. *Lunar Planet. Sci.* **18,** 185–186.

Clayton R. N., Hinton R. W., and Davis A. M. (1988) Isotopic variations in the rock-forming elements in meteorites. *Phil. Trans. R. Soc. Lond. A* **325,** 483–501.

Clayton R. N., Mayeda T. K., Goswami J. N., and Olsen E. J. (1991) Oxygen isotope studies of ordinary chondrites. *Geochim. Cosmochim. Acta* **55,** 2317–2338.

Cohen B. A., Hewins R. H., and Yu Y. (2000) Evaporation in the young solar nebula as the origin of "just-right" melting of chondrules. *Nature* **406,** 600–602.

Cohen B., Hewins R. H., and Alexander C. M. O'D. (2004) The formation of chondrules by open-system melting of nebular condensates. *Geochim. Cosmochim. Acta* **68,** 1661–1675.

Connolly H. C. Jr., Hewins R. H., Ash R. D., Zanda B., Lofgren G. E., and Bourot-Denise M. (1994) Carbon and the formation of reduced chondrules. *Nature* **371,** 136–139.

Connolly H. C. Jr., Huss G. R., and Wasserburg G. J. (2001) On the formation of Fe-Ni metal in Renazzo-like carbonaceous chondrites. *Geochim. Cosmochim. Acta* **65,** 4567–4588.

Cuzzi J. N., Hogan R. C., Paque J. M., and Dobrovolskis A. R. (2001) Size-selective concentration of chondrules and other small particles in protoplanetary nebula turbulence. *Astrophys. J.* **546,** 496–508.

Cuzzi J. N. (2004) Blowing in the wind: III. Accretion of dust rims by chondrule-sized particles in a turbulent protoplanetary nebula. *Icarus*, **168,** 484–497.

Delaney J. S. (1995) Nonthermal initiation of nucleation and chondrule texture development (abstract). *Meteoritics* **30,** 501.

Desch S. J. and Cuzzi J. N. (2000) The generation of lightning in the Solar Nebula. *Icarus* **143,** 87–105.

Desch S. J. and Connolly H. C. Jr. (2002) A model of the thermal processing of particles in solar nebula shocks: Application to the cooling rates of chondrules. *Meteor. Planet. Sci.* **37,** 183–208.

Ebel D. S. and Grossman L. (2000) Condensation in dust-enriched systems. *Geochim. Cosmochim. Acta* **64,** 339–366.

Ebel D. S. and Alexander C. M. O'D. (2002) Origin of enstatite chondrites and implications for the inner planets (abstract 2335). In *Proceedings of the V. M. Goldschmidt Conference.* Cambridge Publications.

Galy A., Young E. D., Ash R. D., and O'Nions R. K. (2000) Formation of chondrules at high gas pressures in the solar nebula. *Science* **290,** 1751–1754.

Ghiorso M. S. and Sack R. O. (1995) Chem. mass transfer in magmatic processes IV. A revised and internally consistent thermodynamic model for the interpretation and extrapolation of liquid-solid equi-

libria in magmatic systems at elevated temperatures and pressures. *Contib. Mineral. Petrol.* **119,** 197–212.

Grossman J. N., Alexander C. M. O'D., Wang J., and Brearley A. J. (2002) Zoned chondrules in Semarkona: Evidence for high- and low-temperature processing. *Meteor. Planet. Sci.* **37,** 49–74.

Grossman J. N. and Brearley J. (2003) Cryptic metamorphic effects in chondrules from highly unequilibrated ordinary chondrites: an insidious parent-body process. *Lunar Planet. Sci.* **34,** 1584.

Grossman L. (1972) Condensation in the primitive solar nebula. *Geochim. Cosmochim. Acta* **36,** 597–619.

Grossman L., Ebel D. S., Simon S. B., Davis A. M., Richter F. M., and Parsad N. M. (2000) Major element chemical and isotopic compositions of refractory inclusions in C3 chondrites: The separate roles of condensation and evaporation. *Geochim. Cosmochim. Acta* **64,** 2879–2894.

Hewins, R. H. (1988) Experimental studies of chondrules. In *Meteorites and the early Solar System* (eds. J. F. Kerridge and M. S. Matthews), pp. 660–679. University of Arizona Press.

Hewins R. H. and Radomsky P. M. (1990) Temperature conditions for chondrule formation. *Meteoritics* **25,** 309–318.

Hewins R. H., Yu Y., Zanda B., and Bourot-Denise M. (1997) Do nebular fractionations, evaporative loss, or both, influence chondrule compositions? *Antarct. Meteorite Res.* **10,** 294–317.

Hsieh K.-C., Vlach K. C., and Chang Y. A. (1987) The Fe-Ni-S system 1. A thermodynamic analysis of the phase equilibria and calculation of the phase diagram from 1173 to 1623 K. *High Temp. Sci.* **23,** 17–38.

Itoh S. and Yurimoto H. (2003) Contemporaneous formation of chondrules and refractory inclusions in the early Solar System. *Nature* **423,** 728–731.

Jones R. H. (1990) Petrology and mineralogy of type II, FeO-rich chondrules in Semarkona (LL3.0): Origin by closed-system fractional crystallization, with evidence for supercooling. *Geochim. Cosmochim. Acta* **54,** 1785–1802.

Jones R. H. (1994) Petrology of FeO-poor, porphyritic pyroxene chondrules in the Semarkona meteorite. *Geochim. Cosmochim. Acta* **58,** 5325–5340.

Jones R. H. (1996) FeO-rich porphyritic pyroxene chondrules in unequilibrated ordinary chondrites. *Geochim. Cosmochim. Acta* **60,** 3115–3138.

Jones R. H. and Scott E. R. D. (1989) Petrology and thermal history of type IA chondrules in the Semarkona (LL3.0) chondrite. *Proc. Lunar Planet. Sci. Conf.* **19,** 523–536.

Jones R. H. and Lofgren G. E. (1993) A comparison of FeO-rich, porphyritic olivine chondrules in unequilibrated chondrites and experimental analogues. *Meteoritics* **28,** 213–221.

Kehm K., Hauri E. H., Alexander C. M. O'D., and Carlson R. W. (2003) High precision iron isotope measurements of meteoritic material by cold plasma ICP-MS. *Geochim. Cosmochim. Acta* **67,** 2879–2891.

Knacke O., Kubaschewski O., and Hesselmann K. (1991) *Thermodynamic Properties of Inorganic Substances.* Springer-Verlag.

Kracher A., Scott E. R. D., and Keil K. (1983) Relict and other anomalous grains in chondrules: Implications for chondrule formation. *J. Geophys. Res.* **89,** B559–B566.

Lange R. A. and Carmichael I. S. E. (1987) Densities of Na_2O-K_2O-CaO-MgO-FeO-Fe_2O_3-Al_2O_3-TiO_2-SiO_2 liquids: New measurements and derived partial molar properties. *Geochim. Cosmochim. Acta* **51,** 2931–2946.

Lofgren G. E. (1996) A dynamic crystallization model for chondrule melts. In *Chondrules and the Protoplanetary Disk* (eds. R. H. Hewins, R. H. Jones, and E. R. D. Scott), pp. 187–196. Cambridge University Press.

Lyons J. R. and Young E. D. (2003) Towards an evaluation of self-shielding at the X-point as the source of the oxygen isotope anomaly in CAIs. *Lunar Planet. Sci.*, **34,** 1981.

MacPherson G. J., Paque J. M., Stolper E., and Grossman L. (1984) The origin and significance of reverse zoning in melilite from Allende Type B inclusions. *J. Geol.* **92,** 289–305.

MacPherson G. J., Davis A. M., and Zinner E. K. (1995) The distribution of aluminum-26 in the early Solar System—A reappraisal. *Meteoritics* **30,** 365–386.

Messenger S. and Walker R. M. (1997) Evidence for molecular cloud material in meteorites and interplanetary dust. In *Astrophysical Implications of the Laboratory Study of Presolar Materials,* Vol. 402 pp. 545–564. (eds. T. Bernatowicz and E. Zinner). Am. Inst. Phys., Woodbury.

Messenger S., Keller L. P., and Walker R. M. (2002) Discovery of abundant interstellar silicates in cluster IDPs. *Lunar Planet. Sci.* **33,** 1887.

Mullane E., Russell S. S., Gounelle M., and Mason T. F. D. (2003) Iron isotope compositions of Allende matrix, CAIs and chondrules. *Meteor. Planet. Sci.* **38,** A66.

Navon O. and Wasserburg G. J. (1985) Self-shielding in O_2—A possible explanation of oxygen isotopic anomalies in meteorites? *Earth Planet. Sci. Lett.* **73,** 1–16.

Nguyen L.-A., Alexander C. M. O'D., and Carlson R. W. (2000) Mg isotope variation in bulk meteorites and chondrules. *Lunar Planet. Sci.* **31,** 1841.

Nittler L., Alexander C. M. O'D., Gao X., Walker R. M., and Zinner E. (1997) Stellar sapphires: The properties and origins of presolar Al_2O_3 in meteorites. *Astrophys. J.* **483,** 475–495.

Nittler L. R., Alexander C. M. O'D., Wang J., and Gao X. (1998) Meteoritic oxide grain from supernova found. *Nature* **393,** 22219.

Palme H., Larimer J. W., and Lipschutz M. E. (1988) Moderately volatile elements. In *Meteorites and the Early Solar System* (eds. J. F. Kerridge and M. S. Matthews), pp. 436–461. University of Arizona Press.

Rambaldi E. R. and Wasson J. T. (1981) Metal and associated phases in Bishunpur, a highly unequilibrated ordinary chondrite. *Geochim. Cosmochim. Acta* **45,** 1001–1015.

Rambaldi E. R. and Wasson J. T. (1984) Metal and associated phases in Krymka and Chainpur: Nebular formational processes. *Geochim. Cosmochim. Acta* **48,** 1885–1897.

Richter F. M., Davis A. M., Ebel D. S., and Hashimoto A. (2002) Elemental and isotopic fractionation of Type B calcium-, aluminum-rich inclusions: Experiments, theoretical considerations and constraints on their evolution. *Geochim. Cosmochim. Acta* **66,** 521–540.

Rubin A. E., Sailer A. L., and Wasson J. T. (1999) Troilite in the chondrules of type-3 ordinary chondrites: Implications for chondrule formation. *Geochim. Cosmochim. Acta* **63,** 2281–2298.

Scott E. R. D. and Taylor G. J. (1983) Chondrules and other components in C, O and E chondrites: Similarities in their properties and origins. *J. Geophys. Res.* **88,** B275–B286.

Sears D. W. G., Huang S., and Benoit P. H. (1996) Open-system behavior during chondrule formation. In *Chondrules and the Protoplanetary Disk* (eds. R. H. Hewins, R. H. Jones, and E. R. D. Scott), pp. 221–232. Cambridge University Press.

Sheng Y. J., Hutcheon I. D., and Wasserburg G. J. (1991) Origin of plagioclase-olivine inclusions in carbonaceous chondrites. *Geochim. Cosmochim. Acta* **55,** 581–599.

Shu F. H., Shang H., and Lee T. (1996) Toward an astrophysical theory of chondrites. *Science* **271,** 1545–1552.

Shu F. H., Shang H., Glassgold A. E., and Lee T. (1997) X-rays and fluctuating X-winds from protostars. *Science* **277,** 1475–1479.

Shu F. H., Shang H., Gounelle M., Glassgold A. E., and Lee T. (2001) The origin of chondrules and refractory inclusions in chondritic meteorites. *Astrophys. J.* **548,** 1029–1050.

Stolper E. (1982) Crystallization sequences of Ca-Al-rich inclusions from Allende: An experimental study. *Geochim. Cosmochim. Acta* **46,** 2159–2180.

Stolper E. and Paque J. (1986) Crystallization sequences of Ca-Al-rich inclusions from Allende: The effects of cooling rate and maximum temperature. *Geochim. Cosmochim. Acta* **50,** 1785–1806.

Thiemens M. H. (1988) Heterogeneity in the nebula: Evidence from stable isotopes. In *Meteorites and the Early Solar System* (eds. J. F. Kerridge and M. S. Matthews), pp. 899–923. University of Arizona Press.

Thiemens M. H. (1999) Mass-independent isotope effects in planetary atmospheres and the early solar system. *Science* **283,** 341–345.

Wang J., Davis A. M., Clayton R. N., Mayeda T. K., and Hashimoto A. (2001) Chemical and isotopic fractionation during the evaporation of the FeO-MgO-SiO_2-CaO-Al_2O_3-TiO_2 rare earth element melt system. *Geochim. Cosmochim. Acta* **65,** 479–494.

Wark D. A. (1987) Plagioclase-rich inclusions in carbonaceous chondrite meteorites: Liquid condensates? *Geochim. Cosmochim. Acta* **51,** 221–242.

Wasson J. T. (1993) Multiplicity of chondrule heating events and the coarsening of chondrule textures. *Lunar Planet. Sci.* **24,** 1489–1490.

Weston R. E. Jr. (1999) Anomalous or mass-independent isotope effects. *Chem. Rev.* **99,** 2115–2136.

Wood J. A. and Hashimoto A. (1993) Mineral equilibrium in fractionated nebular systems. *Geochim. Cosmochim. Acta* **57,** 2377–2388.

Woolum D. S. and Cassen P. (1999) Astronomical constraints on nebular temperatures: Implications for planetesimal formation. *Meteor. Planet. Sci.* **34,** 897–908.

Xiong Y. and Hewins R. H. (2000) Experimental determination of evaporation rates of iron and palladium under nebular conditions and their implications (abstract). *Meteor. Planet. Sci.* **35,** A172–A173.

Xiong Y. and Hewins R. H. (2001) Experimental determination of evaporation rates and coefficients of metallic nickel under nebula conditions (abstract). *Meteor. Planet. Sci.* **36,** A227.

Yoneda S. and Grossman L. (1995) Condensation of CaO-MgO-Al_2O_3-SiO_2 liquids from cosmic gases. *Geochim. Cosmochim. Acta* **59,** 3413–3444.

Young E. D. and Russell S. S. (1998) Oxygen reservoirs in the early solar nebula inferred from an Allende CAI. *Science* **282,** 452–455.

Young E. D. and Lyons J. R. (2003) CO self shielding in the outer solar nebula: An astrochemical explanation for the oxygen isotope slope-1 line. *Lunar Planet. Sci.* **33,** 1923.

Yu Y. and Hewins R. H. (1997) Evaporation of potassium and sodium under vacuum conditions—Did chondrules really form at low pressure? *Lunar Planet. Sci.* **28,** 1613–1614.

Yurimoto H. and Kuramoto K. (2002) A possible senario introducing heterogeneous oxygen isotopic distribution in protoplanetary disks. *Meteor. Planet. Sci.* **37,** A153.

Zanda B., Bourot-Denise M., Perron C., and Hewins R. H. (1994) Origin and metamorphic redistribution of silicon, chromium and phosphorous in the metal of chondrites. *Science* **265,** 1846–1849.

Zhu X. K., Guo Y., O'Nions R. K., Young E. D., and Ash R. D. (2001) Isotopic homogeneity of iron in the early solar nebula. *Nature* **412,** 311–313.